

International Atomic Energy Agency

INDC(CCP)-135/LN

---

**INDC**

**INTERNATIONAL NUCLEAR DATA COMMITTEE**

---

Translations of Contributed Soviet Papers

Submitted to the May 1979 IAEA Advisory Group Meeting

on Transactinium Nuclear Data

August 1979

---

IAEA NUCLEAR DATA SECTION, KÄRNTNER RING 11, A-1010 VIENNA

Reproduced by the IAEA in Austria  
August 1979

Translations of Contributed Soviet Papers  
Submitted to the May 1979 IAEA Advisory Group Meeting  
on Transactinium Nuclear Data

August 1979



Table of Content

Neutron data requirements for calculating transactinide isotope build-up in reactors, Yu.G. Bobkov, A.S. Krivtsov, L.N. Usachev, V.E. Kolesov . . . . .	1
Measurements and evaluations of nuclear data on actinide isotopes, V.M. Kulakov, L.L. Sokolovskij . . . . .	11
Investigation of neutron resonances of $^{247}\text{Cm}$ in the 0.5 - 20 eV energy range T.S. Belanova, A.G. Kolesov, A.V. Klinov, S.N. Nikol'skij, V.A. Poruchikov, V.N. Nefedov, V.S. Artamonov, R.N. Ivanov, S.M. Kalebin . . . . .	23
New measurements of partial decay half-lives of the isomeric state of $^{242\text{m}}\text{Am}$ A.G. Zelenkov, V.A. Pchelin, Yu.F. Rodionov, L.V. Chistyakov, V.M. Shubko . . . . .	25
Half-life of the $(1/2)^+$ -isomer of $^{235}\text{U}$ V.I. Zhudov, V.M. Kulakov, B.V. Odinov . . . . .	27
Conversion electron spectrum of the $(1/2)^+$ isomer of $^{235}\text{U}$ V.I. Zhudov, A.G. Zelenkov, V.M. Kulakov, V.I. Mostovoj, B.V. Odinov . . . . .	35
Comparison of various theoretical models based on neutron $^{242}\text{Pu}$ cross section calculations V.A. Konshin . . . . .	43



79-4271  
Translated from Russian

NEUTRON DATA REQUIREMENTS FOR CALCULATING TRANSACTINIDE  
ISOTOPE BUILD-UP IN REACTORS

Yu.G. Bobkov, A.S. Krivtsov, L.N. Usachev  
and V.E. Kolesov

1. An approach to determining the necessary accuracies for nuclear data

References [1-2] outline an approach to the quantitative determination of the necessary accuracies for nuclear data based on a generalized theory of perturbations and on non-linear programming. This approach was applied in Ref. [3] to the problem of determining the necessary accuracies for transactinide isotope data. Its essential features are described below. The necessary accuracies for nuclear data  $d_{ir}$  ( $i = 1 \dots N$ ) should: (a) be such as to give the accuracies  $H_j$  ( $j = 1 \dots L$ ) required for calculation of transactinide isotope build-up in the reactor; (b) be better than, or equal to, the accuracies  $d_{ia}$  ( $i = 1 \dots N$ ) already attained; (c) be obtainable at minimum cost. On the basis of the foregoing, the quantities  $d_{ir}$  are determined from the solution of the following extremum problem:

$$F = \sum_{i=1}^N \lambda_i / d_{ir}^2 \rightarrow \min \quad 1A$$

$$\sum_{i=1}^N S_{ij}^2 d_{ir}^2 \leq H_j^2 \quad (j = 1 \dots L) \quad 1B$$

$$d_{ir} \leq d_{ia} \quad (i = 1 \dots N) \quad 1C$$

In accordance with the convention that has developed, the quantities  $S_{ij}$  are called sensitivity coefficients. They are used to establish a linear relationship between the relative variations of constants  $(\delta\sigma/\sigma)_i$  and the resulting relative variations  $\delta C/C$  of the calculated parameters

$$\delta C/C = \sum_i S_{ic} (\delta\sigma/\sigma)_i \quad (a)$$

This problem is solved by the method of non-linear programming in combination with special programs [4].

## 2. Calculation of the sensitivity coefficients

The sensitivity coefficients  $S_{ij}$  entering into conditions of type 1B are calculated by the theory of perturbations for evolutionary problems, which also include the problem of burn-up calculation. This theory of perturbations for linear functionals was formulated for the first time by Gandini [5] and then used, generalized and developed further in Refs [6-8]. The equations for the higher orders of the theory of perturbations and for the fractional linear functionals are given in Refs [9-10]. The coefficients  $S_{ij}$  for various types of reactors and irradiation conditions are given in Refs [11-14]. To calculate these coefficients we used the PERS program [15]. Comparison of the coefficients obtained by this program with those of similar nature from the above-mentioned references shows reasonable agreement. As an example Table 1 gives the sensitivity coefficients for the calculated quantities of  $^{238}\text{Pu}$  and  $^{236}\text{Pu}$  in the blankets of a fast reactor and fusion reactor containing only  $^{238}\text{U}$  and in the core of a fast reactor containing higher Pu isotopes and also those of  $^{232}\text{U}$  in a fusion reactor blanket.

## 3. Attained and required accuracies for transactinide nuclear data

At present it appears to be difficult to make reliable evaluations of the accuracies attained in the nuclear data for most transactinides, except in the case of  $^{235}\text{U}$ ,  $^{239}\text{Pu}$ ,  $^{240}\text{Pu}$  and  $^{238}\text{U}$ . For one thing, the various evaluations of particular elements have not been compared sufficiently fully and, for another, the error ascribed to certain experiments is much smaller than the divergences between the different experiments and evaluations. Problems of calculating isotope build-up always involve cross-sections averaged over the spectrum of the apparatus studied. For this reason, when we henceforth refer to accuracy, both attained and required, we shall mean the accuracy of the cross-section averaged over the spectrum. This may create additional difficulties in formulating the requirements for the accuracy of measurements and evaluations of cross-sections. Some evaluations of the attained accuracies of cross-sections are given in Ref. [16] and also in Ref. [3]. Table 2, column "a", gives the evaluations of the attained accuracy of cross-sections used in our present work.

Assuming that the errors of the different cross-sections are not corrected (or considering the correlations to be low), we can evaluate the accuracy of calculation  $D_j$  ( $j = 1 \dots L$ ) of the build-up of the different isotopes in the reactor and in the blanket for the formula

$$D_j^2 = \sum_{i=1}^N S_{ij}^2 d_{ia}^2 \quad (b)$$

The accuracies of build-up calculation thus evaluated are given in Table 3. The main column shows the error component resulting only from nuclear data while the figures in brackets also take into account the error in the neutron flux, assumed to be equal to 10%. The values of the required cross-section accuracies (substantially within the framework of problem (1)) depend on the required accuracies of build-up calculation. These accuracies follow from a consideration of the isotopic composition of fast reactor fuel and its influence on the external fuel cycle [17]. At present we can hardly expect an accurate formulation of these requirements. In the present study we have taken two variants - one (1) with more moderate requirements and the other (2) with more rigorous ones. Accordingly, we have obtained two versions of cross-section accuracy requirements: these are given in Table 2 in column "r" with figures (1) and (2), respectively. In our opinion, these figures limit the possible upper and lower ranges of the requirements for cross-section accuracy.

#### 4. Discussion of the requirements obtained

The most important requirements are those put forward with respect to the cross-sections of (n,2n) reactions in the case of the isotopes  $^{238}\text{U}$  and  $^{237}\text{Np}$  and to the capture cross-sections for a number of elements ( $^{240}\text{Pu}$ ,  $^{241}\text{Pu}$ ,  $^{242}\text{Pu}$  and  $^{243}\text{Am}$ ). The requirements for the fission cross-sections are, on the whole, not far off from those already attained.

The rigorous requirements as regards the fission cross-sections of the (n,2n) reaction give rise to additional accuracy requirements in calculating the part of the reactor spectrum lying above the threshold of the (n,2n) reaction. Obviously, this problem calls for special study.

The situation is apparently most serious in the case of the average cross-section of the (n,2n) reaction for  $^{237}\text{Np}$ . We know that a number of evaluations of the cross-section for this reaction averaged over the fast

reactor spectrum differ from one another by a factor of up to 4-5, and this should lead to still greater differences in the evaluations of accumulated  $^{236}\text{Pu}$ . This is significant also in the case of fast reactors, where the absolute magnitude of  $^{236}\text{Pu}$  build-up is comparatively small. However, this is of special significance in the case of the fusion blanket, where the  $^{236}\text{Pu}$  and  $^{238}\text{Pu}$  build-up exceeds by a factor of 100-1000 the corresponding build-up of these elements in the fast reactor blanket and core for the same quantities of accumulated  $^{239}\text{Pu}$ .

Extensive build-up of these isotopes may create a number of additional difficulties in the reprocessing of this kind of fuel. Moreover, some studies published in connection with the International Nuclear Fuel Cycle Evaluation point out that a larger build-up of these isotopes gives rise to additional safeguards problems for the nuclear fuel.

As regards the necessary accuracies for nuclear data in respect of transactinide build-up in a fusion reactor blanket, the situation here is as follows: isotopes beyond  $^{240}\text{Pu}$  do not in practice accumulate in the blanket and therefore the requirements which are formulated for capture and fission cross-sections on the basis of fast reactor requirements are sufficient for the fusion reactor. As for the calculation of the build-up of  $^{236}\text{Pu}$ ,  $^{238}\text{Pu}$  and some other isotopes, it will be seen from Table 1 that the values of the sensitivity coefficients for the fast and fusion reactor blankets practically coincide. Therefore, the requirements for the cross-sections averaged over the spectrum of the corresponding blanket coincide quantitatively when the requirements for the accuracy of build-up calculation are identical. The difference between these requirements will be due to the fact that they are formulated for other spectrum regions which are shifted towards higher energies.

##### 5. Formulation of requirements in particular energy intervals

The requirements given in Table 2 are formulated for cross-sections averaged over the reactor spectrum. If we consider that the errors in the cross-section are fully correlated (i.e. they are systematic) in a region of the energy spectrum, these requirements can then be regarded as requirements for systematic error in cross-section determination.

If the energy axis can be sub-divided into "m" intervals within which the errors in the cross-section are correlated but where there is no

correlation between the intervals, the requirements for the accuracy of determining cross-sections in a particular interval  $d_k$  ( $k = 1, \dots, m$ ) can be obtained in the same way as in Ref. [1] for a reactor parameter. Here the part of such a reactor parameter will be played by the average cross-section  $\langle \sigma \rangle$  and that of the constants by the cross-section in the  $k$ -th energy interval  $\sigma_k$ . The following quantities are used as the sensitivity coefficients:

$$S_k = \sigma_k F_k / \sum_i \sigma_i F_i = \sigma_k F_k / \langle \sigma \rangle \quad (c)$$

Here  $F_k$  is the neutron flux in the  $k$ -th interval used in the averaging of the cross-sections. It is assumed that this flux is normalized to unity. It logically follows that the quantities  $S_k$  represent the contribution of the cross-section of the  $k$ -th interval to the total cross-section of the process.

According to the algorithm described in Ref. [1], the optimum accuracy required in the  $k$ -th interval  $d_k$  is determined in terms of the required accuracy of the cross-section  $d_r$  and the quantity  $S_k$  in the following manner:

$$d_k = d_r / (\sqrt{S_k} \sum_i S_i) = d_r / \sqrt{S_k} \quad (d)$$

This formula can be applied on the assumption that the relative costs of measuring the cross-sections in different intervals are identical and that the error in the average cross-section is due only to the given cross-section and contains no component connected with inaccuracy of the spectrum.

## 6. Conclusion

Preliminary analysis shows that the nuclear data accuracies that have been attained do not provide the accuracies necessary for calculating build-up in fast reactors. A good deal of work has to be done on the measurement and evaluation of a large number of  $(n, 2n)$  reaction and capture cross-sections.

It is also necessary to refine the accuracies necessary for build-up calculation, from the standpoint of fuel reprocessing and fabrication technology and reuse of fuel in reactors.

It is of interest to study the correlations between the build-up of the various isotopes [3] in order to see whether the measurements of the build-up of certain isotopes can be used to refine the build-up calculations for others and thus to lower the accuracy requirements for nuclear data.

Integral measurements of the ratios of reaction rates in different critical assemblies also contain much information.

Table 1

Sensitivities of the calculated quantities of  $^{232}\text{U}$ ,  $^{236}\text{Pu}$  and  $^{238}\text{Pu}$  build-up in fast and fusion reactor blankets and in a fast reactor core

	Fast reactor blanket		Fusion reactor blanket			Fast reactor core	
	$^{236}\text{Pu}$	$^{238}\text{Pu}$	$^{232}\text{U}$	$^{236}\text{Pu}$	$^{238}\text{Pu}$	$^{236}\text{Pu}$	$^{238}\text{Pu}$
$^{236}\text{Pu}$ $\lambda_\alpha$	-0.09		0.934	-0.09		-0.09	
$^{236}\text{Pu}$ $(n, \gamma)$	-0.01		-0.004	-0.005	-0.00	-0.05	
$^{236}\text{Pu}$ $(n, f)$	-0.01		-0.004	-0.005		-0.05	
$^{236}\text{Np}$ $\lambda_{\beta^-}$	0.433		0.434	0.433		0.433	
$^{236}\text{Np}$ $\lambda_{\beta^+}$	-0.425		-0.425	-0.425		-0.425	
$^{237}\text{Np}$ $(n, 2n)$ I			I	I		I	
$^{237}\text{Np}$ $(n, \gamma)$	-0.047	0.823	-0.015	-0.02	0.91	-0.19	0.47
$^{238}\text{U}$ $(n, 2n)$ I		0.86	I	I	0.92	I	0.58
$^{238}\text{U}$ $(n, \gamma)$		+0.13			+0.07	-0.04	
$^{239}\text{Pu}$ $\lambda_{\beta^-}$	0.043	0.038	0.06	0.04		0.043	0.025
$^{239}\text{Pu}$ $(n, 2n)$		0.14			0.076		0.23
$^{242}\text{Cm}$ $\lambda_\alpha$		$2 \cdot 10^{-5}$			$3,4 \cdot 10^{-7}$		0.11
$^{238}\text{Np}$ $\lambda_{\beta^-}$		0.012			0.013		
$^{238}\text{Pu}$ $(n, f)$		-0.04			-0.016		-0.17
Integral flux	I.9	I.88	1.9	1.9	1.9		



Table 3

Accuracies attained and required in calculating  
transactinide build-up

Isotope	Accuracy required		Accuracy attained	
	1	2	Fast reactor shield	Fast reactor core
Pu - 236	30	15	100	100
Pu - 238	20	10	50	35
Pu - 240	5	2	12(22)	4.5(5)
Pu - 241	4	2	25(37)	6.5(8)
Pu - 242	10	5	30(50)	9(9)
Am - 241	5	3	25(37)	6.5(9)
Am - 242	20	10	30(47)	18 (18)
Am - 243	20	10	60(77)	47 (48)
Cm - 242	20	10	30(48)	13 (14)
Cm - 244	30	15	70(98)	67 (70)

REFERENCES

- [1] USACHEV, L.N., BOBKOV, Yu.G., Planning of the optimum set of micro-experiments and evaluations satisfying the accuracy requirements for reactor parameter calculation (in Russian), INDC (CCP) 19/U, IAEA, Vienna (1972).
- [2] BOBKOV, Yu.G., PYATNITSKAYA, L.T., USACHEV, L.N., Planning of experiments and evaluations for reactor neutron data (in Russian), INDC (CCP) 46/L, IAEA, Vienna (1974).
- [3] USACHEV, L.N., BOBKOV, Yu.G., KOLESOV, V.E., KRIVTSOV, A.S., "Determination of the required accuracies of transactinide neutron data for calculation of their build-up in fast reactors" (in Russian). Proceedings of the International Conference on Nuclear Data, Harwell (1978).
- [4] BOBKOV, Yu.G., USACHEV, L.N., "Problems of nuclear data" (in Russian) in: Yadernye konstanty (Nuclear Constants) No. 16, Atomizdat, Moscow (1976).
- [5] GANDINI, A., Nucl. Sci. Eng. 38 1 (1969).
- [6] KHROMOV, V.V., KASHUTIN, A.A., GLEBOV, V.G., "The linear theory of perturbations in the problems of fuel burn-up in fast reactors" (in Russian), At.Ehnerg. 1 (1974) 59.
- [7] KRUGLOV, A.K., RUDIN, A.P., Artificial Protons and the Method of Calculating Their Formation in Fast Reactors (in Russian), Atomizdat, Moscow (1976).
- [8] GANDINI, A., Nucl. Sci. Eng. 59, 60 (1976).
- [9] BOBKOV, Yu.G., GRUZD, S.M., KRIVTSOV, A.S., KOLESOV, V.E., The theory of perturbations for polynomial models in problems of the evolutionary type (in Russian). Preprint FEhI-871, Obninsk (1978).
- [10] GANDINI, A., Nucl. Sci. Eng. 67 3 (1979).
- [11] GANDINI, A., OLIVA, G., TONDINELLI, L., Correlation between irradiation experimentals and nuclear data for actinide production assessment. CNEN, RT/FI(77)1.
- [12] KUGTERS, H., LALOVIC, M., Transactinium isotope build-up and decay in reactor fuel and related sensitivity to cross-section change. In TND, v.1, IAEA-186, Vienna, 1976, p. 139.

- [13] BARRE, I.Y., BOUCHARD, I., Importance of transactinide nuclear data for physics of fast and thermal reactor cores. In TND, v.1, p. 113.
- [14] MITANI, H., KOYAMA, K., KUROI, H., Sensitivity analysis of build-up and decay of actinides in fast reactors. Paper submitted to the NEACRP, 21st meeting, Tokai, November 1978.
- [15] BOBKOV, Yu.G., KRIVTSOV, A.S., "The PERS program" in: Nuclear Physics Research in the USSR (in Russian), Atomizdat, Moscow (1978).
- [16] Report of the Working Group on the requirements of TND for fast reactors. Report of the Working Group on the requirements of TND in waste management. In TND v.1, IAEA-186, Vienna, 1976, p. 17-28.
- [17] BAKULENKO, O.D., IKHLOV, E.M., KULAKOVSKIJ, M.Ya., ROMASHKIN, V.G., TROYANOV, M.F., TSYKUNOV, A.G., "The physical characteristics of fast reactor fuel and their influence on the fuel cycle" (in Russian), At. Ehnerg. 44 (1978) 140.

MEASUREMENTS AND EVALUATIONS OF NUCLEAR DATA ON  
ACTINIDE ISOTOPES

(Review of papers published by Soviet scientists during 1975-1978)

V.M. Kulakov and L.L. Sokolovskij  
I.V. Kurchatov Institute of Atomic Energy, Moscow (1979)

## I. MEASUREMENTS OF DECAY DATA

Uranium-235

The spectrum of the gamma radiation accompanying  $^{235}\text{U}$  and  $^{231}\text{Th}$  radioactive decay has been studied with precision semiconductor detectors. The spectrum revealed 102 gamma lines, many of which were found for the first time. A refined energy level scheme for  $^{231}\text{Th}$  has been constructed from experimental data [1].

Uranium-235 (isomer)

The differential spectrum of the conversion electrons of the  $(\frac{1}{2}^+)$ -isomer of  $^{235}\text{U}$  has been measured with a modified Hewlett-Packard HP 5950A electron spectrometer for chemical analysis. The spectrum showed lines corresponding to conversion on the  $6p_{\frac{1}{2}}$ ,  $6p_{3/2}$  and  $6d$  electron shells of the uranium atom. The isomer excitation energy was determined as  $(76 \pm 2)$  eV.

A method has been developed for accumulation of the  $(\frac{1}{2}^+)$ -isomer of  $^{235}\text{U}$  during the alpha decay of  $^{239}\text{Pu}$  and a technique devised for detection of low-energy conversion electrons. An apparatus to measure the half-life of the isomer has been designed. The isomer half-life was found to be  $25.0 \pm 0.5$ ,  $26.8 \pm 0.7$  and  $26.5 \pm 0.7$  min for accumulation on gold, uranium dioxide and uranium tetrafluoride substrates, respectively [3].

Plutonium-238

The isotope formed as a result of alpha-decay of  $^{242}\text{Cm}$  was used, after careful radiochemical purification, for determination of the half-life of  $^{238}\text{Pu}$ . The isotopic composition, as determined in a mass spectrometer, was as follows:  $^{238}\text{Pu} - (99.82 \pm 0.02)$ ,  $^{239}\text{Pu} - (0.08 \pm 0.02)$  and  $^{240}\text{Pu} - (0.10 \pm 0.02)$  at.%. The radiochemical purity of the plutonium was verified by alpha- and gamma-spectrometry, which did not reveal any foreign alpha emitters in the plutonium preparation. The half-life of  $^{238}\text{Pu}$  measured by the  $4\pi\alpha$  method was:  $T_{\frac{1}{2}} = 86.98 \pm 0.39$  a (at 95% confidence level) [4].

Plutonium-239

The difference between the  $^{239}\text{Pu}$  half-life measurements by radiometric and calorimetric methods has been analysed [5] and found to constitute 1-1.5% for 0.1-0.2% measurement errors. The work was based on the use

of the radiometric method, the accuracy and reliability of which were improved by coulometric weighing of the plutonium, and the activity of the preparations was measured by the  $4\pi\alpha$ -X coincidence method. The measured half-life of  $^{239}\text{Pu}$  was  $(24\,060 \pm 38)$  a at 95% confidence level.

Americium-241

The half-life of  $^{241}\text{Am}$  has been determined by the method of  $4\pi\alpha$  measurements of a solution with a known concentration of the isotope under study.  $^{241}\text{Am}$  accumulated in  $^{241}\text{Pu}$  decay was used in the work. The  $^{241}\text{Am}$  dioxide contained ~ 2%  $^{237}\text{Np}$ , 0.16%  $^{239}\text{Pu}$  and not more than 2% inert impurities. The measured half-life of  $^{241}\text{Am}$  was  $432.8 \pm 3.1$  a at 95% confidence level [6].

Americium-243

The half-life has been measured in two  $^{243}\text{Am}$  samples having different isotopic compositions [7]. The characteristics of the samples are given in Table 1.

Table 1

	Sample 1	Sample 2
Content of inert impurities, wt%	$\leq 0.3$	$\leq 0.5$
Impurities of foreign alpha-emitters, % of total alpha-activity	$\leq 0.1$	$\leq 0.09$
Mass spectrum, at. %		
$^{241}\text{Am}$	$3.379 \pm 0.050$	$0.524 \pm 0.019$
$^{243}\text{Am}$	$96.621 \pm 0.050$	$99.476 \pm 0.019$
Alpha-spectrum, % of total alpha-activity		
$^{241}\text{Am}$	$37.39 \pm 0.47$	$7.98 \pm 0.30$
$^{243}\text{Am}$	$62.61 \pm 0.47$	$92.02 \pm 0.30$

The mass-spectrometric analysis of each sample was performed three times in the mass range from 238 to 244, and masses other than those mentioned in Table 1 were not found. The alpha-spectrometric measurements were carried out with a silicon detector. The weighted mean half-life of  $^{243}\text{Am}$  from measurements on two samples was  $7380 \pm 34$  a (at 95% confidence level).

The absolute values of gamma quantum yield in  $^{243}\text{Am}$  alpha-decay has been determined with a high degree of accuracy [8]. The following half-life values were used in the calculations:  $^{243}\text{Am}$  half-life  $7380 \pm 34$  a and  $^{241}\text{Am}$  half-life  $432.8 \pm 3.1$  a.

#### Curium-245

The  $^{245}\text{Cm}$  alpha-decay has been measured with a magnetic alpha-spectrograph [9]. A curium source enriched with  $^{245}\text{Cm}$  was used for the measurements. Ten alpha groups have been recorded and the level scheme for  $^{241}\text{Pu}$  constructed.

#### Curium-246

The half-life of  $^{246}\text{Cm}$  has been determined by two methods: (1) from the molar concentration ratios of  $^{246}\text{Cm}$  and  $^{244}\text{Cm}$  and of  $^{240}\text{Pu}$  and  $^{242}\text{Pu}$  formed in their decay; and (2) from the specific activity of  $^{246}\text{Cm}$  measured by the method of  $4\pi\alpha$  counting with isotopic dilution. In both cases, the half-life of  $^{246}\text{Cm}$  was determined in relation to that of  $^{244}\text{Cm}$ , the value of which was taken as  $18.099 \pm 0.015$  a [10]. The weighted mean half-life of  $^{246}\text{Cm}$  was  $4852 \pm 76$  a at 95% confidence level [11].

#### Berkelium-245

The alpha-spectrum of  $^{245}\text{Bk}$  obtained in the reaction  $^{243}\text{Am}(\alpha, 2n)$  has been studied on an enriched  $^{243}\text{Am}$  isotope. Sixteen groups of the fine structure of alpha radiation were recorded and the energy level schemes for  $^{241}\text{Am}$  constructed [12].

#### Berkelium-249

The half-life of  $^{249}\text{Bk}$  has been determined by the radiometric method. The activity was measured over a period of one year using an end-window counter with 0.5% accuracy. The stability of the apparatus was verified with a  $^{14}\text{C}$  preparation. The  $^{249}\text{Bk}$  half-life was found to be  $325 \pm 7$  d. The maximum beta-particle energy of  $^{249}\text{Bk}$  was measured. The maximum energy determined by a Curie plot was  $123 \pm 3$  keV and that determined by the absorption method  $124 \pm 3$  keV [13].

The alpha-decay of  $^{249}\text{Bk}$  was studied with a magnetic alpha-spectrograph. The energies and intensities of 10 alpha groups were determined [14].

#### Californium-249

For  $^{249}\text{Cf}$  half-life measurement two samples were used: (1) mono-isotopic, radiochemically pure  $^{249}\text{Cf}$  obtained from  $^{249}\text{Bk}$  decay; and

(2) a mixture of heavy californium isotopes from which Bk, Cm and other elements had been removed [15]. The weighted mean half-life of  $^{249}\text{Cf}$  was found to be  $366 \pm 6$  a at 95% confidence level.

## II. EVALUATION OF THE RADIOACTIVE PROPERTIES OF NUCLIDES OF MASS 242

The Atomic and Nuclear Data Centre of the USSR State Committee on the Utilization of Atomic Energy has evaluated the radioactive properties of nuclides of mass 242 [16]. A critical evaluation has been made of half-lives, level energies, beta- and gamma-transition energies and intensities for isobars with  $A = 242$ . The evaluation also included new data on the spontaneously fissionable isomers in this group of nuclei. The mean values at the final stage of evaluation (after analysis and sorting of data) were calculated by the method described in Ref. [17].

The following results were obtained for specific nuclides:

### Plutonium-242

The weighted mean half-lives of  $^{242}\text{Pu}$  were:

$$T_{\frac{1}{2}} (\alpha \text{ } ^{242}\text{Pu}) = 3.761(11) \times 10^5 \text{ a}$$

$$T_{\frac{1}{2}} (\text{spont. fiss. } ^{242}\text{Pu}) = 6.86(17) \times 10^{10} \text{ a}$$

The  $^{242}\text{Pu}$  energy levels are excited in  $^{242}\text{Am}$  electron capture and  $^{246}\text{Cm}$  alpha-decay.

The evaluated characteristics for  $^{242}\text{Am}$  electron capture are given in Table 2.

Table 2

E level	$E_{\text{EC}}$ (keV)	$I_{\text{EC}}$ (%)	$E_{\gamma}$ (keV)	$I_{\text{conv.el.}}$ (per 100 decays)	Internal conversion coefficient
0	752(5)	6			
44.539(7)	707(5)	11	44.539(7)	11	761

Total decay energy  $Q_{\beta} = 752(5)$  keV.

In the case of  $^{246}\text{Cm}$  alpha-decay, the total decay energy was evaluated:  $Q_{\alpha} = 5475(2)$  keV. The evaluated half-life ( $\alpha \text{ } ^{246}\text{Cm}$ ) was  $4.772(36) \times 10^3$  a. The energy levels of  $^{242}\text{Pu}$  were evaluated on the basis of the results of nuclear reaction studies.

Americium-242

The ground state of  $^{242}\text{Am}$  decays in two ways: by electron capture to  $^{242}\text{Pu}$  and by  $\beta^-$ -decay to  $^{242}\text{Cm}$ .

The evaluated characteristics of the ground state are:

$$T_{\frac{1}{2}} = 16.010(15) \text{ h}$$

Ratio of the probabilities of decay  $\beta^-/\text{EC} = 4.96(9)$

$$I_{\beta} = 83.2(3)\% - \text{calculated from the ratio } \beta^-/\text{EC}$$

$$I_{\text{EC}} = 16.8(3)\% - \text{calculated from the ratio } \beta^-/\text{EC}$$

Quadrupole electric moment  $Q = -2.7 \text{ b}$

Magnetic moment  $M = +0.3802(15)$

The isomeric state of  $^{242}\text{Am}$  decays in three ways:

- (1) Gamma transition to the ground state of  $^{242}\text{Am}$ ;
- (2) Weak alpha-decay to  $^{238}\text{Np}$ ;
- (3) Spontaneous fission.

The isomeric state characteristics taken are:

$$E_x = 48.63(6) \text{ keV}$$

Total half-life  $T_{\frac{1}{2}} = 152(7) \text{ a}$ .

$$T_{\frac{1}{2}} (\alpha \text{ } ^{242}\text{Am}) = 3.20(16) \times 10^4 \text{ a}$$

Relative probability of alpha-decay - 0.476(14)%.

The energy level values of  $^{242}\text{Am}$  were evaluated.

Curium-242

The evaluated values of the lifetime of the  $^{242}\text{Cm}$  ground state are:

$$T_{\frac{1}{2}} (\alpha \text{ } ^{242}\text{Cm}) = 162.75(3) \text{ d}$$

$$T_{\frac{1}{2}} (\text{spont. fiss. } ^{242}\text{Cm}) = 7.2(2) \times 10^6 \text{ a}$$

The energy levels of  $^{242}\text{Cm}$  have been evaluated from the  $^{246}\text{Cf}$  alpha-decay data. For  $^{246}\text{Cf}$  the following have been evaluated: total alpha-decay energy  $Q_{\alpha} = 6861.3(10) \text{ keV}$  and half-life  $T_{\frac{1}{2}} (\alpha \text{ } ^{246}\text{Cf}) = 35.7(5) \text{ h}$ .

Berkelium-242

There are practically no data on the  $^{242}\text{Bk}$  ground state. The information on the levels of  $^{242}\text{Bk}$  has been obtained from the alpha-decay of  $^{246}\text{Es}$ . The evaluated characteristics of the  $^{246}\text{Es}$  alpha-decay are:

$$T_{\frac{1}{2}} (\alpha \text{ } ^{246}\text{Es}) = 7.7(5) \text{ min}$$
$$E_{\alpha} = 7345(18) \text{ keV}$$

The relative probability of alpha-decay is 9.9(15)%.

Californium-242

The evaluated half-life is  $T_{\frac{1}{2}} = 3.49(12)$  min. The ground state of  $^{242}\text{Cf}$  is reached by alpha-transition (100%) with energy  $E_{\alpha} = 8238(9)$  keV from the ground state of  $^{246}\text{Fm}$ .

Evaluated  $T_{\frac{1}{2}} (^{246}\text{Fm}) = 1.28(12)$  s.

Fermium-242

The value of  $T_{\frac{1}{2}} (^{242}\text{Fm})$  was taken as  $0.8(2) \times 10^{-3}$  s.

III. REACTIONS WITH NEUTRONS

(a) Fission reaction

The fragment mass distributions in  $^{232}\text{Th}$  fission induced by 1.2-3.0 MeV neutrons have been measured. The fine structure of the fragment mass distribution appears clearly at a neutron energy of 1.2 MeV but becomes less pronounced as energy increases [18]. The angular anisotropy has been measured for pairs of fragments of symmetric and asymmetric masses in  $^{232}\text{Th}$  fission induced by neutrons of  $E_n = 3$  MeV. It has been established that the angular anisotropy is identical within measurement errors in both methods of fission [19].

The fission cross-sections for  $^{233}\text{U}$  and  $^{235}\text{U}$  have been measured in relation to the cross-section for the reaction  $^{10}\text{B}(n,\alpha)^7\text{Li}$  for 2 keV neutrons separated from the reactor neutron spectrum by a 960 mm long scandium filter. The cross-section values obtained are  $(7.54 \pm 0.17)$  b for  $^{233}\text{U}$  and  $(6.19 \pm 0.12)$  b for  $^{235}\text{U}$  [20].

The cross-sections of  $^{233}\text{U}$  fission induced by 0.0253 eV and 2, 24, 55 and 144 keV neutrons have been measured at the CM-2 reactor (Scientific Research Institute for Atomic Reactors, Dimitrovgrad). A double ionization chamber was used for the measurements. The fission cross-sections of  $^{233}\text{U}$  were measured in relation to those of  $^{235}\text{U}$  measured earlier with 2% accuracy. For the above neutron energies the fission cross-sections obtained are  $528.6 \pm 8.0$ ,  $8.93 \pm 0.22$ ,  $2.94 \pm 0.08$ ,  $2.45 \pm 0.06$  and  $2.16 \pm 0.05$  b, respectively [21].

The cross-sections of fission induced by fast neutrons (up to 7.5 MeV) for  $^{233}\text{U}$ ,  $^{238}\text{U}$ ,  $^{239}\text{Pu}$ ,  $^{240}\text{Pu}$ ,  $^{241}\text{Pu}$  and  $^{242}\text{Pu}$  have been measured in relation to the  $^{235}\text{U}$  fission cross-section. The measurements were carried out on an electrostatic generator, the reactions  $\text{Li}(p,n)$ ,  $\text{T}(p,n)$  and  $\text{D}(d,n)$  having been used as neutron sources. The double ionization chamber served as the fission fragment detector [22].

Absolute measurements have been made of the 14.8 MeV neutron-induced fission cross-sections of  $^{237}\text{Np}$  and  $^{239}\text{Pu}$  by the method of fission coincidences in a target of the isotope under study with the particles accompanying the neutrons. The measurement accuracy was better than 2%. The neutron source was a neutron generator based on the reaction  $^3\text{H}(d,n)^4\text{He}$ . The fission cross-sections were determined from the ratio of the number of coincidences and the number of alpha-particles. The following cross-section values were obtained [23]:

	$\sigma_f, \text{ b}$
$^{233}\text{U}$	$2.350 \pm 0.042$
$^{237}\text{Np}$	$2.430 \pm 0.047$
$^{239}\text{Pu}$	$2.620 \pm 0.046$

For the same isotopes absolute measurements have been performed for the cross-sections of fission induced by  $^{252}\text{Cf}$  fission-spectrum neutrons; the method used was based on coincidences between the fission fragments of the isotope under study and those of  $^{252}\text{Cf}$  [24]. The measurement error was 1.6%.

The following values were obtained:

	$\sigma_f, \text{ mb}$
$^{233}\text{U}$	$1947 \pm 31$
$^{237}\text{Np}$	$1442 \pm 23$
$^{239}\text{Pu}$	$1861 \pm 30$

The work was carried out with the support of the IAEA (research contract No. 1718/RB).

The time-of-flight technique was used to measure the prompt neutron spectra of  $^{233}\text{U}$ ,  $^{235}\text{U}$  and  $^{239}\text{Pu}$  fission induced by thermal neutrons in the 0.01-4 MeV region and  $^{252}\text{Cf}$  spontaneous fission in the 0.01-10 MeV region [25]. The time resolution was 2.5-3 ns. The neutrons were recorded with thresholdless detectors based on  $^{235}\text{U}$  with no sensitivity to gamma quanta.

The ratios of the mean energies of neutrons emitted in  $^{233}\text{U}$ ,  $^{235}\text{U}$  and  $^{239}\text{Pu}$  fission and  $^{252}\text{Cf}$  spontaneous fission were measured with a multi-channel macroscopic spectrometer. The measurements were carried out in a BR-10 reactor. The  $^{252}\text{Cf}$  spontaneous fission neutron spectrum was used as the standard. The following ratios were obtained:  $(0.967 \pm 0.003) : (0.946 \pm 0.003) : (0.983 \pm 0.002) : 1$  [26].

The prompt neutron spectra of  $^{240}\text{Pu}$ ,  $^{244}\text{Cm}$  and  $^{252}\text{Cf}$  spontaneous fission were measured in one experiment under the same conditions. The values of the spectrum hardness parameter obtained were 1.26, 1.33 and 1.42 MeV, respectively [27].

The fast fission cross-section of  $^{244}\text{Pu}$  has been measured on an electrostatic accelerator [28]. The reaction  $\text{T}(p,n)^3\text{He}$  served as the neutron source. It has been established that the energy dependence of the cross-section is of the threshold type. The fission threshold is  $E_n = 0.75$  MeV and barrier height 5.5 MeV. The cross-section at the plateau is 1.1 b, which is substantially higher than that expected from systematics based on allowance for  $z$  and  $A$  of fissionable nuclei.

The time-of-flight method was used to measure the  $^{252}\text{Cf}$  spontaneous fission neutron spectrum in the 0.01-10 MeV region [29]. The neutron detector was an ionization chamber with 12 layers of  $^{235}\text{U}$  mixed oxide having a diameter of 10 cm and total material amounting to 1.5 g. It was found that in the measured energy range the experimental results agreed satisfactorily, within the limit of experimental error, with a Maxwellian distribution having parameter  $T = 1.41 \pm 0.03$  MeV. The fine structure was investigated in the  $^{252}\text{Cf}$  spontaneous fission neutron spectrum in the 1-5 MeV energy range. No irregularities were discovered in the spectrum within experimental errors (1.5-2.5%) [30].

Measurements have been made of the yields of the  $^{252}\text{Cf}$  binary and ternary fission neutrons at angles of  $0^\circ$  and  $90^\circ$  to the direction of fragment divergence [31]. The following neutron yield values were obtained (in relative units):

Table 3

	$0^\circ$	$90^\circ$
Binary fission	1	$0.231 \pm 0.005$
Ternary fission	$1.03 \pm 0.15$	$0.155 \pm 0.028$

(b) Other reactions

The resonance-averaged total neutron cross-sections and scattering cross-sections of  $^{235}\text{U}$  for 2 keV neutrons were determined in the WWR-M reactor by means of a scandium filter. The value of  $\alpha = (\bar{\sigma}_t - \bar{\sigma}_s - \bar{\sigma}_f) / \bar{\sigma}_f$  for  $\bar{\sigma}_f = 6.3 \pm 0.13$  b was found to be  $0.55^{+0.09}_{-0.06}$  [32].

The spectra of the secondary neutrons generated in  $^{238}\text{U}$  bombardment by neutrons with an initial energy of  $9.1 \pm 0.2$  MeV have been measured on the 150-cm cyclotron of the Institute of Physics and Power Engineering by the time-of-flight technique at angles of  $30^\circ$ ,  $60^\circ$ ,  $90^\circ$ ,  $120^\circ$  and  $150^\circ$ . The double differential cross-sections of the interaction of neutrons with  $^{238}\text{U}$  nuclei were determined. The integral spectrum of neutrons from the reactions  $(n, n')$  and  $(n, 2n)$  has been analysed in terms of the pre-equilibrium model [33].

The partial neutron inelastic-scattering cross-sections for the  $2^+$ ,  $4^+$ ,  $1^-$  and  $3^-$  states and also the differential cross-sections of elastic scattering at  $90^\circ$  for the  $^{238}\text{U}$  nucleus in the 0.68–1.4 MeV neutron range have been determined by the time-of-flight method in a pulsed electrostatic accelerator [34].

The time-of-flight method was used for CM-2 reactor measurements of the total neutron cross-section of  $^{242}\text{Cm}$  in the 1–265 eV energy region and for determination of the neutron resonance parameters [35]. The measurements were made by means of a neutron chopper with magnetic suspension of rotors. The following were determined from the experimental data:

average distance between levels  $\bar{D} = 17.6 \pm 3.3$  eV; average reduced neutron width  $\bar{\Gamma}_0 = 1.1 \pm 0.5$  MeV; neutron strength function  $S_0 = (0.64 \pm 0.32) \times 10^{-4}$ . The resonance integral  $I = 115 \pm 53$  b was determined from the level parameters.

The total cross-sections of  $^{244}\text{Cm}$ ,  $^{245}\text{Cm}$ ,  $^{246}\text{Cm}$  and  $^{248}\text{Cm}$  have been determined on the CM-2 reactor by the time-of-flight method [36]. The resonance parameters were calculated by the shape and area method using the single-level Breit-Wigner formula. A better resolution of the spectrometer at 92 m path length was 90 ns/m. In the measurements the statistical accuracy was kept within 0.5-1.5%; the neutron background did not exceed 4%.

A microtron bremsstrahlung beam was used to measure the photofission yields of  $^{232}\text{Th}$ ,  $^{233}\text{U}$ ,  $^{235}\text{U}$ ,  $^{236}\text{U}$ ,  $^{238}\text{U}$ ,  $^{237}\text{Np}$ ,  $^{239}\text{Pu}$ ,  $^{241}\text{Pu}$  and  $^{241}\text{Am}$  nuclei in the 4.4-7.0 MeV region and of  $^{232}\text{Th}$ ,  $^{236}\text{U}$ ,  $^{238}\text{U}$  and  $^{237}\text{Np}$  nuclei in the deep sub-barrier energy region of 3.5-4.6 MeV [37]. The sources of the background have been analysed in detail. The resonance structure of the cross-sections and the effects of the double-humped fission barrier are discussed and a comparison made of the fissionability of nuclei in the reactions  $(\gamma, f)$ ,  $(n, f)$  and in direct reactions.

The relative photofission probabilities of  $^{235}\text{U}$ ,  $^{238}\text{U}$ ,  $^{237}\text{Np}$ ,  $^{239}\text{Pu}$ ,  $^{241}\text{Am}$  and  $^{243}\text{Am}$  nuclei in the 100-1000 MeV energy region of gamma quanta have been measured in 300 and 2000 MeV linear electron accelerators. The fission fragments were recorded by glass detectors. The photofission yields obtained for the above nuclei at the maximum bremsstrahlung gamma energies were 100, 240, 400 and 1200 MeV [38].

REFERENCES

- [1] BARANOV, S.A., SHATINSKIJ, V.M. et al. *Yad. Fiz.* 26, 5 (1977) 921.
- [2] ZHUDOV, V.I., ZELENKOV, A.G. et al. Abstracts of Papers Presented at the 29th All-Union Meeting on Nuclear Spectroscopy and the Structure of the Atomic Nucleus, Riga (1979) (in Russian).
- [3] ZHUDOV, V.I., KULAKOV, V.M., ODINOV, B.V., Abstracts of Papers Presented at the 29th All-Union Meeting on Nuclear Spectroscopy and the Structure of the Atomic Nucleus, Riga (1979) (in Russian).
- [4] POLYUKHOV, V.G. et al., *At. Ehnerg.* 40, 1 (1976) 61.
- [5] ALEKSANDROV, B.M. et al., *Izv. Akad. Nauk SSSR, Ser. Fiz.* 39, 3 (1975) 482.
- [6] POLYUKHOV, V.G. et al., *At. Ehnerg.* 36, 4 (1974) 319.
- [7] POLYUKHOV, V.G., et al., *At. Ehnerg.* 37, 4 (1974) 357.
- [8] STAROZHUKOV, D.I. et al., *At. Ehnerg.* 42, 4 (1977) 319.
- [9] BARANOV, S.A., SHATINSKIJ, V.M., *Yad. Fiz.* 22, 4 (1975) 670.
- [10] BENTLEY, W.C., *J. Inorg. Nucl. Chem.*, 30, 8 (1968) 2007.
- [11] POLYUKHOV, V.G. et al., *Radiokhimiya* 19, 4 (1977) 507.
- [12] BARANOV, S.A., SHATINSKIJ, V.M. et al., *Yad. Fiz.* 21, 1 (1975) 230.
- [13] GLAZOV, V.M. et al., *At. Ehnerg. Pis'ma* 37, 1 (1974) 78.
- [14] BARANOV, S.A., SHATINSKIJ, V.M., *Zh. Ehksp. Teor. Fiz.* 68, 1 (1975) 8.
- [15] POLYUKHOV, V.G. et al., *Radiokhimiya* 19, 4 (1977) 460.
- [16] GRIGOR'YAN, Yu.I., CHUKREEV, F.E., SHURSHIKOV, E.N., Abstracts of Papers Presented at the 28th All-Union Meeting on Nuclear Spectroscopy and the Structure of the Atomic Nucleus (Alma-Ata) Nauka, Leningrad (1978) 556 (in Russian).
- [17] GRIGOR'YAN, Yu.I., SOKOLOVSKIJ, L.L., CHUKREEV, F.E., Rep. INDC (CCP) - 75/L.N., IAEA, Vienna.
- [18] D'YACHENKO, N.P. et al., Proceedings of the Fourth Conference on Neutron Physics (Kiev, April 1977), TsNII Atominform, Moscow, Part 3 (1977) 171.

- [19] VOROB'EVA, V.G. et al., *ibid.*, Part 3, p. 183.
- [20] MURZIN, A.V. et al., *ibid.*, Part 2, p. 252.
- [21] ZHURAVLEV, K.D. et al., *ibid.*, Part 3, p. 131.
- [22] FURSOV, B.N. et al., *ibid.*, Part 3, p. 144.
- [23] ALKHAZOV, I.D. et al., *ibid.*, Part 3, p. 155.
- [24] ADAMOV, V.M. et al., *ibid.*, Part 3, p. 158.
- [25] NEFEDOV, V.N. et al., *ibid.*, Part 3, p. 205.
- [26] BOL'SHOV, V.I. et al., *ibid.*, Part 3, p. 284.
- [27] ALEKSANDROVA, Z.A. et al., *At. Ehnerg.* 36, 4 (1974).
- [28] HOCHBERG, B.M. et al., *Yad. Fiz.* 25, 1 (1977).
- [29] BLINOV, M.V. et al., Proceedings of the Fourth Conference on Neutron Physics (Kiev), TsNII Atominform, Moscow, Part 3 (1977) 197.
- [30] BATENKOV, O.I. et al., *ibid.*, Part 3, p. 201.
- [31] ANDREJCHUK, L.M. et al., *ibid.*, Part 3, p. 230.
- [32] GNIDAK, N.L. et al., *ibid.*, Part 2, p. 223.
- [33] BIRYUKOV, N.S. et al., *ibid.*, Part 2, p. 22.
- [34] VOROTNIKOV, P.E. et al., *ibid.*, Part 2, p. 119.
- [35] ARTAMONOV, V.S. et al., *ibid.*, Part 2, p. 257.
- [36] BELANOVA, T.S. et al., *ibid.*, Part 2, p. 260.
- [37] ZHUCHKO, V.E. et al., *Yad. Fiz.* 28, 5 (1978) 1170, 1185.
- [38] ALEKSANDROV, B.M. et al., *Yad. Fiz.* 28, 5 (1978) 1165.

INVESTIGATION OF NEUTRON RESONANCES OF  
 $^{247}\text{Cm}$  IN THE 0.5-20 eV ENERGY RANGE

Belanova, T.S., Kolesov, A.G., Klinov, A.V., Nikol'ski j, S.N.,  
Poruchikov, V.A., Nefedov, V.N., Artamonov, V.S., Ivanov, R.N.,  
Kalebin, S.M.

The neutron resonance parameters of  $^{247}\text{Cm}$  were calculated from the transmission of a curium sample measured by the time-of-flight method. The measurements were performed in a horizontal neutron beam from the SM-2 reactor. The neutron pulse was formed by a mechanical selector with three rotors suspended in a magnetic field [1]. The path length of the spectrometer was 91.7 m and the best resolution 120 ns/m.

The sample investigated was made from a powder of stable curium oxide ( $\text{Cm}_2\text{O}_3$ ) calcined at 900-1100°C with known oxygen content. The impurities included  $^{243}\text{Am}$  and  $^{240}\text{Pu}$ , the latter accumulating in the sample as a result of decay of  $^{244}\text{Cm}$ . The maximum content of  $^{247}\text{Cm}$  at the time of measurement was  $0.64 \times 10^{-4}$  at./b. The content of inert impurities apart from oxygen did not exceed 3%. Transmission was measured in the 0.5-20 eV neutron energy range with a statistical error of 1-2% at the tails of the resonance. The neutron background did not amount to more than 2% of the effect.

The neutron resonance parameters were calculated by the shape method using the single-level Breit-Wigner formula [1]. Since the neutron resonance parameters of  $^{244}\text{Cm}$ ,  $^{245}\text{Cm}$ ,  $^{246}\text{Cm}$ ,  $^{248}\text{Cm}$ ,  $^{243}\text{Am}$  and  $^{240}\text{Pu}$  are well known [2-6], it was possible to identify the neutron resonances of  $^{247}\text{Cm}$  from the measured transmission and calculate their parameters (see table). In Refs [3, 5-6] the neutron resonances of  $^{247}\text{Cm}$  with energies of 1.247, 3.19 and 18.1 eV are erroneously assigned to  $^{245}\text{Cm}$ . A neutron resonance with an energy of 2.919 eV had not been previously detected.

We identified only five neutron resonances of  $^{247}\text{Cm}$  with high values of  $2g\Gamma_n$ . This is due to the fact that the  $^{247}\text{Cm}$  content of the sample is low (1.7 mg) and the resonances of this isotope are identified against the background of a large number of resonances of  $^{244}\text{Cm}$ ,  $^{245}\text{Cm}$ ,  $^{246}\text{Cm}$ ,  $^{248}\text{Cm}$ ,  $^{243}\text{Am}$  and  $^{240}\text{Pu}$  situated in the energy range in question.

Table  
Neutron resonance parameters of  $^{247}\text{Cm}$

$E_0$ , eV	$\Gamma$ , meV	$2g_n^2$ , meV
$1.247 \pm 0.005$	$74 \pm 4$	$0.56 \pm 0.09$
$2.919 \pm 0.010$	$70 \pm 30$	$0.10 \pm 0.04$
$3.189 \pm 0.010$	$103 \pm 6$	$1.0 \pm 0.1$
$9.55 \pm 0.03$	$166 \pm 60$	$0.91 \pm 0.33$
$18.1 \pm 0.1$	$210 \pm 170$	$3.7 \pm 1.5$

REFERENCES

- [1] BELANOVA, T.S. et al., Atomic Reactor Research Institute preprint, NIIAR P-6 (272) Dimitrovgrad (1976).
- [2] Neutron Cross-sections, BNL-325, Third Ed. 1973, Vol. 1.
- [3] BELANOVA, T.S. et al., At. Ehnerg. 42 1 (1977) 52.
- [4] BENJAMIN, R.W. et al., Nucl. Sci. Eng. 55 4 (1974).
- [5] BELANOVA, T.S. et al., in Trudy konf. "Nejtronnaya fizika" (Proc. Conf. "Neutron physics") izdat TsNIIatominform pt 3 (1976) 224.

---

Translator's Note: Ref. [6] not supplied.

79-04274

Translated from Russian

NEW MEASUREMENTS OF PARTIAL DECAY HALF-LIVES  
OF THE ISOMERIC STATE OF  $^{242m}\text{Am}$

Zelenkov, A.G., Pchelin, V.A., Rodionov, Yu.F.,  
Chistyakov, L.V., Shubko, V.M.

ABSTRACT

The half-life of the isomer  $^{242m}\text{Am}$  and the partial alpha decay half-life were measured and found to be  $141 \pm 2$  years and  $(3.12 \pm 0.05) \times 10^4$  years respectively.

---

In recent years the need has arisen to refine actinide element nuclear data, to meet the requirements of nuclear power engineering and various branches of nuclear industry[1], this applying in particular to the half-lives of the transplutonium elements[2, 3]. One nuclide which needs to be studied more thoroughly is the long-lived isomer of  $^{242}\text{Am}$ , the lifetime and partial alpha-decay half-life of which have been measured only once 20 years ago[4], being found to be  $152 \pm 7$  years and  $(3.20 \pm 0.16) \times 10^4$  years respectively.

We undertook repeat measurements of the above quantities in order to check and refine the results obtained. A product highly enriched in the nuclide concerned was used for the measurements.

Determining the partial alpha-decay half-life is fairly simple, the procedure being to compare the mass ratio of  $^{242m}\text{Am}$  and  $^{241}\text{Am}$  in the product with the alpha spectrum measured with the aid of semiconductor spectrometers and a magnetic alpha-spectrograph. The value obtained was  $(3.12 \pm 0.05) \times 10^4$  years. A half-life for  $^{241}\text{Am}$  of  $432.6 \pm 0.6$  years was used in the determination[3].

The total lifetime of  $^{242m}\text{Am}$  was measured by two methods. Four series of measurements of the accumulation of  $^{242}\text{Cm}$  formed as a result of beta disintegration of  $^{242m}\text{Am}$  were carried out on the freshly purified product, using a semiconductor alpha-spectrometer.

The rate of accumulation of alpha activity of  $^{242}\text{Cm}$  with respect to the alpha activity of  $^{242\text{m}}\text{Am}$  was found to be  $(3.22 \pm 0.04) \times 10^{-2}$  1/h. From this the half-life of  $^{242\text{m}}\text{Am}$  was determined as:

$$T_{\frac{1}{2}}(^{242\text{m}}\text{Am}) = 141.9 \pm 1.7 \text{ years}$$

A half-life for  $^{242}\text{Cm}$  of  $(162.8 \pm 0.4 \text{ days})$ [3] and a beta decay branching ratio for  $^{242}\text{Am}$  of  $(83 \pm 0.5)\%$ [5, 6] were used in the calculation.

To determine the half-life of  $^{242\text{m}}\text{Am}$ , we also performed measurements of the ratio between the alpha-intensity and the total intensity of the conversion and beta radiation of  $^{242\text{m}}\text{Am}$  and  $^{242}\text{Am}$ . The measurements were performed using proportional  $4\pi$  -counters. In order to attain maximum soft radiation recording efficiency, the product was coated onto thin gold films. A correction was made for the accumulation of  $^{242}\text{Cm}$  measured at the same time with a semiconductor alpha-spectrometer. Measurements were carried out on seven targets made of the freshly purified product. The ratio of the total intensity of the conversion and beta radiation of  $^{242\text{m}}\text{Am}$  and  $^{242}\text{Am}$  to the alpha intensity of  $^{242\text{m}}\text{Am}$  was found to be  $431 \pm 6$ , from which a value of  $T_{\frac{1}{2}}(^{242\text{m}}\text{Am}) = 139.7 \pm 1.8$  years was obtained. In making this calculation, it was assumed that the relative intensity of electron capture of  $^{242}\text{Am}$  to the ground state is  $(6.5 \pm 0.3)\%$ [5, 6], and the fluorescence yield 0.96.

On the basis of these measurements we recommend that a half-life for  $^{242\text{m}}\text{Am}$  of  $141 \pm 2$  years be adopted, together with a relative probability of alpha disintegration of  $(0.45 \pm 0.01)\%$ . We do not regard the values obtained as contradicting the results of Ref.[4] but rather as refinements thereof. The situation is understandable considering the significant change that has occurred over the last 20 years in the values of the half-lives of  $^{241}\text{Am}$  and  $^{243}\text{Am}$  used in calculations.

#### REFERENCES

1. Transactinium Isotope Nuclear Data (TND) Proceedings of an Advisory Group Meeting held in Karlsruhe, 3-7 November 1975, Report OAEA-186.
2. BARANOV, S.A., ZELENKOV, A.G., KULAKOV, V.M., paper in Ref.[1]; also At. Ehnerg. 41 (1976) 342.
3. Summary report of first Co-ordinated Research Meeting on the Measurement of Transactinium Isotope Nuclear Data. INDC (NDS) report 96/N, IAEA, Vienna (1978).
4. BARNERS, R.F. et al., J. Inorg. Nucl. Chem. 2 (1959) 105.
5. CHUKREEV, F.E., GRIGOR'YAN, Yu.I., SHURSHIKOV, E.N., Abstracts of the 28th Conference on nuclear spectroscopy and the structure of the nucleus (1978) 556.
6. ENSDF (1977).

Paper presented at the 29th Conference on nuclear spectroscopy  
and the structure of the atomic nucleus (Riga, 1979)

HALF-LIFE OF THE  $(1/2)^+$ -ISOMER OF  $^{235}\text{U}$

V.I. Zhudov, V.M. Kulakov, B.V. Odinov

Key words: uranium, isomer, half-life

ABSTRACT

The apparatus and methodology developed for measuring the half-life of the  $(1/2)^+$ -isomer of  $^{235}\text{U}$  are described. Methods of accumulating the isomer and the technique for detecting low-energy conversion electrons are discussed. For accumulation of the isomer on gold, uranium dioxide and uranium tetrafluoride bases the half-lives obtained were  $25.0 \pm 0.5$  min,  $26.8 \pm 0.7$  min and  $26.5 \pm 0.7$  min respectively.

---

The decay of the "26-minute"  $(1/2)^+$ -isomer of uranium-235 ( $^{235}\text{U}^m$ ) represents a unique case of conversion of the nuclear E3 transition [1, 2] by the outer atomic electron shells. The energy of excitation of the isomer is only  $\sim 76$  eV [3]. The  $(6 p_{1/2})^2$ ,  $(6 p_{3/2})^4$  and  $6 d$  electron shells of uranium participate in the conversion. Perturbation of these shells in chemical compounds or as a result of introducing  $^{235}\text{U}^m$  as an impurity atom into the lattice of a solid leads to appreciable changes in the decay constant ( $\lambda$ ) of the isomer [4, 5]. Such information is of particular interest for explaining certain features of the process of conversion of low-energy nuclear transitions. However, in order to obtain reliable experimental data on the "effects" of a variation in  $\lambda$  of  $^{235}\text{U}^m$ , special methods of accumulating the isomer and recording its decay are required [6] together with reliable means of monitoring the chemical composition of the materials under investigation. Bearing in mind these requirements, we devised a system for measuring the decay constant  $\lambda$  of  $^{235}\text{U}^m$  on the basis of an HP 5950A X-ray-electron spectrometer [7].

The isomer can be obtained as a product of natural alpha decay of  $^{239}\text{Pu}$ . Preparation of pure  $^{235}\text{U}^{\text{m}}$  samples by chemical separation of uranium from plutonium is rather difficult owing to the relatively short half-life of the isomer. A simpler way of preparing samples is to collect uranium recoil atoms from a thin layer of plutonium. Collection can be done in a vacuum or in an inert gas atmosphere. In the former case recoil atoms are implanted in a base layer of the material under investigation by means of their residual kinetic energy (up to  $\sim 90$  keV), while in the latter case they are slowed down in the gas and deposited on the surface of the layer with the aid of the electrostatic field. We used both methods of collection. For preparing samples in a vacuum, a  $^{239}\text{Pu}$  source with an area of  $\sim 1$  cm<sup>2</sup> and a surface density of  $\sim 25$   $\mu\text{g}/\text{cm}^2$  was used. Collection was performed in plane-parallel geometry conditions. The source and the base layer were almost in contact with each other. The  $^{235}\text{U}^{\text{m}}$  samples had an effective area of  $10 \times 12$  mm<sup>2</sup> and a maximum initial activity of  $10^2$  disintegrations per second. Preparation of samples by electrostatic collection of recoil nuclei of uranium was performed in spherical geometry conditions. A layer of  $^{239}\text{Pu}$  was deposited by thermal atomization in a vacuum on the internal surface of a platinum hemisphere with a diameter of 80 mm. The thickness of the layer in this case too was  $\sim 25$   $\mu\text{g}/\text{cm}^2$ . The base layer of the material under investigation was placed at the centre of the hemisphere. The isomer was collected on the surface of the base layer in a helium atmosphere at a pressure of  $\sim 0.5$  atm. and a negative potential of the plutonium layer of  $\sim 3$  kV with respect to the potential of the base layer. The corona discharge current was limited to 1 ma. The  $^{235}\text{U}^{\text{m}}$  samples had an effective area of  $5 \times 2$  mm<sup>2</sup> and an initial activity of up to  $\sim 10^5$  disintegrations per second. As well as for measuring  $\lambda$ , we also used samples with this activity ( $10^5$  d./sec) for measuring the differential spectrum of conversion electrons of  $^{235}\text{U}^{\text{m}}$  [3]. Even with careful polishing of the samples the low-energy component predominates in the spectrum, due apparently to scattering of conversion electrons in the material of the samples and to secondary electron emission. This indicates considerable diffusion of the atoms of the isomer during the electrostatic collection of  $^{235}\text{U}^{\text{m}}$ . Consequently,

under favourable conditions for isotopic exchange, one can expect to obtain the desired atomic environment of the isomer by the above two methods of preparing  $^{235}\text{U}^{\text{m}}$  samples. Plutonium impurity was not observed in the samples, this being checked from the alpha activity.

Figure 1 is a photograph of the HP 5950A spectrometer. In the foreground can be seen the prechamber which is used for preparing and cleaning samples investigated by the X-ray-electron spectroscopy method. The vacuum equipment of the spectrometer provides oil-free evacuation of the prechamber up to  $10^{-8}$  torr. The lock system of the spectrometer (not shown on the photograph) enables samples to be introduced rapidly into the prechamber and then into the main chamber of the spectrometer with practically no loss of vacuum in either. The samples can be prepared and their surfaces cleaned directly in the prechamber by means of the thermal atomizer (TA) and the argon ion gun (A) respectively. In addition to these items we installed an isomer accumulator (IA) and a conversion electron detector (CED) in the prechamber. The isomer accumulator is designed for preparation of  $^{235}\text{U}^{\text{m}}$  samples in a vacuum. It comprises a  $^{239}\text{Pu}$  source, a shielded container and a high-vacuum sylphon drive for moving the source. During collection of the isomer the source is moved almost right up to the base layer of the investigated material, and on completion of the collection operation, it is moved back into the container without loss of the vacuum in the chamber. For detecting conversion electrons we used a VEhU-6 open channel secondary-emission multiplier [8]. The latter has a low inherent noise level ( $\sim 0.5$  pulses per sec), a high multiplication factor ( $\sim 10^8$ ) and can operate under saturated signal conditions. The supply voltage of the VEhU-6 in our experiments was  $\sim 3.2$  kV.

Figure 2 is a block diagram of the system for measuring  $\lambda$  of  $^{235}\text{U}^{\text{m}}$ . At the top of the diagram is the prechamber of the HP 5950A spectrometer together with the items mentioned above. The samples (S) of  $^{235}\text{U}^{\text{m}}$  are located at the centre of a section of the chamber. Electrons generated during the decay of the sample are accelerated to 150 V and impinge on the input side of the detector (D). The signals from the detector output are amplified by a linear charge-sensitive circuit (PA, LA), discriminated by an integral discriminator ( $\text{ID}_1$ ) and fed into a 1024-channel pulse analyser ( $\text{PA}_2$ ), which performs on-line recording of the decay curve of the isomer (accumulation of counts, channel by channel). The recording time for each channel is 5 sec. The analyser is connected to the computer of the

HP 5950A (DPS) and to a two-co-ordinate potentiometer (X-Y) by means of which the processing and graphic output of the decay curve are performed. The linear discriminator (LD), the amplitude analyser (AI<sub>1</sub>) and the potentiometer recorder (PR) are used for periodic checking of the conditions of operation of the detector by measuring the spectrum of its output signals. The integral discriminator (ID<sub>2</sub>) and the ratemeters (R<sub>1</sub>, R<sub>2</sub>) are used for checking the functioning of the detector by comparing the counting rate of conversion electrons at different discriminating thresholds of the detector output signals.

The decay constant of the isomer was measured in the following way. Before the isomer was collected, the chemical composition of the surface of the base layer was checked by the X-ray-electron spectroscopy method. If necessary, the surface was cleaned of oxides and sorbed impurities by bombarding the base layer with argon ions. Then the isomer was collected on the base layer and the decay curve was measured. On completion of the measurements the X-ray-electron spectrum of the base layer was recorded again. Figure 3 shows a typical decay curve of <sup>235</sup>U<sup>m</sup> in the ordinary and logarithmic (x 1000) scales. The sample was prepared by vacuum implantation of the isomer in a gold base. Similar measurements were performed for cases where the isomer was deposited electrostatically on UO<sub>2</sub> and UF<sub>4</sub> bases. The decay curves were processed on the HP 2100A computer by the least-squares method on the assumption of a single half-life. For bases of Au, UO<sub>2</sub> and UF<sub>4</sub> we obtained half-lives of 25.0 ± 0.5, 26.8 ± 0.7 and 26.5 ± 0.7 min respectively.

The authors wish to thank Messrs. D.P. Grechukhin, A.A. Soldatov, A.G. Zelenkov and V.I. Mostovoj for their useful suggestions and for their constant interest in the work, and Messrs. A.I. Leonov, V.A. Pchelin and V.M. Shatinskij for their assistance with the experiments.

#### REFERENCES

1. F. Asaro, I. Perlman, *Phys. Rev.*, 107, 318, (1957).
2. J.R. Huizenga, C.L. Rao and D.W. Engelkemeir, *Phys. Rev.*, 107, 319, 195.
3. ZHUDOV, V.I. et al., these proceedings.
4. M. Nève de Mévergnies, *Phys. Rev. Letters*, 29, 1188, 1972.
5. M. Nève de Mévergnies, *Phys. Letters*, 49B, 428, (1974).
6. M. Nève de Mévergnies, *Nuclear Instr. and Meth.*, 109, 145, 1973f.
7. M.A. Kelly, C.E. Tyler, *HP Journal*, July 1973r., p.2.
8. AJNBUND, M.R. et al., in "Elektronnaya tekhnika" (Electronic engineering), series 4, issue No. 9 (1975) 46.

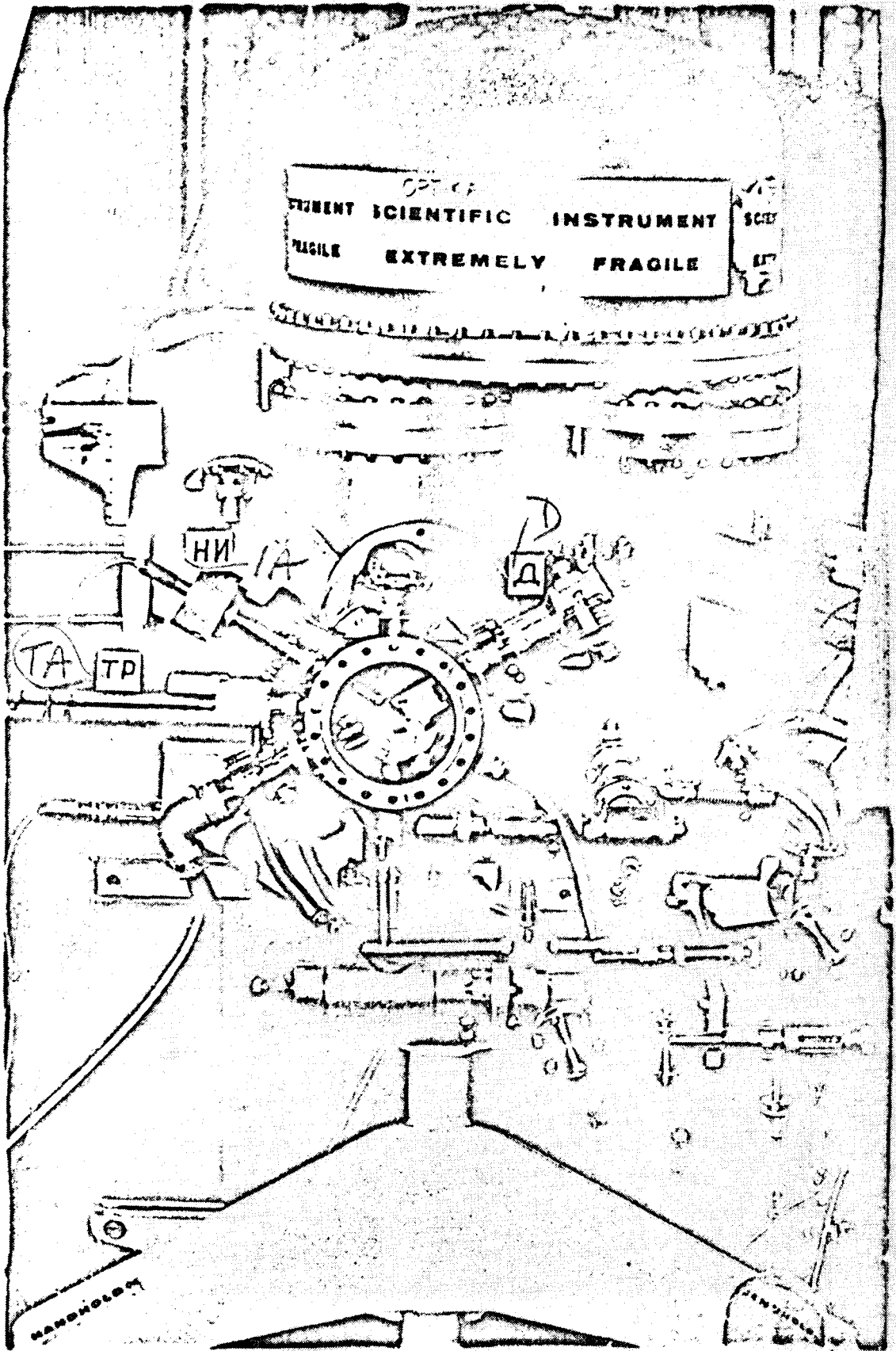
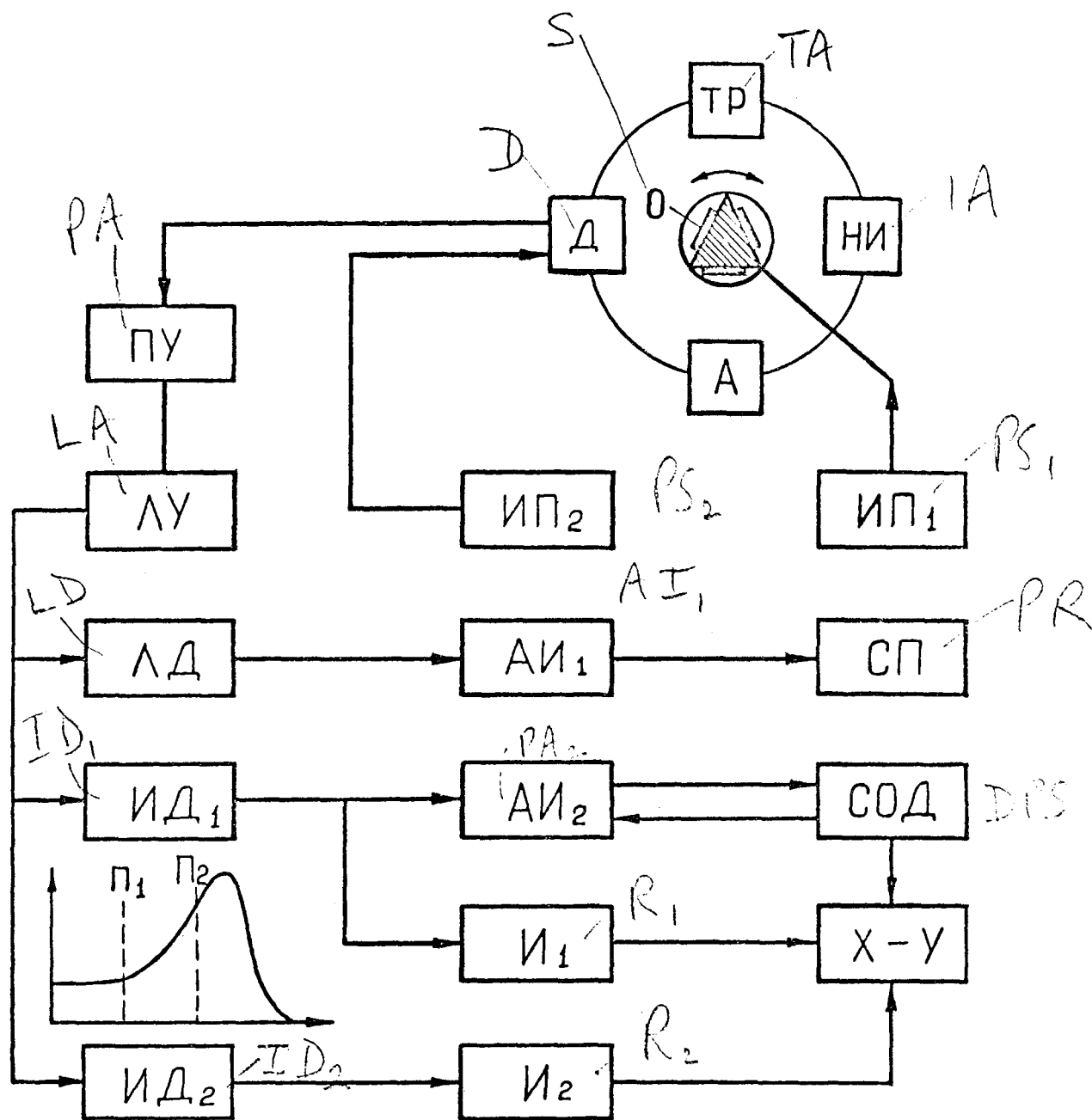


Fig. 1. HP 5950A spectrometer



**Fig. 2.** Block diagram of system for measuring the decay rate of  $^{235}\text{U}$ .  
 O =  $^{235}\text{U}$  sample; TA = thermal atomizer; A = argon ion gun;  
 IA = isomer accumulator ( $^{239}\text{Pu}$ ); D = VEhU-6 conversion electron  
 detector; PA = preamplifier; LA = linear amplifier; LD = linear  
 discriminator; AI<sub>1</sub> = amplitude analyser; PR = potentiometer recorder;  
 ID<sub>1</sub>, ID<sub>2</sub> = integral discriminators; R<sub>1</sub>, R<sub>2</sub> = ratemeters; PA<sub>2</sub> = pulse  
 analyser; DPS = data processing system; X-Y = two-co-ordinate  
 potentiometer; PS<sub>1</sub> = accelerating voltage source; PS<sub>2</sub> = power  
 supply for VEhU-6.

28.10.76.

Measurement of  $\lambda$  of  $^{235}\text{U}^m$  on gold.  
 Collection of  $^{235}\text{U}^m$  in a vacuum at voltage of 600 V.  
 Pressure in chamber  $P = 10^{-6}$  torr.  
 Initial activity  $N_0 = 360 \pm 72$  counts per sec.  
 Background  $70 \pm 14$  counts per sec.  
 Detector VEHU - N 615,  $I_1 = 3.0$  kV.  
 Operating conditions of electronics (?) ..... (?)  
 Discrimination - nil.  
 Curve 1 = decay curve of  $^{235}\text{U}^m$  (80).  
 Curve 2 = ditto in log. scale (1000 ln).  
 Decay constant found by least-squares method.  
 $\lambda = (4.52359 \pm 0.00012) \times 10^{-4} \text{ sec}^{-1}$ ,  $E\lambda = 2.6 \times 10^{-3} \%$ .  
 $T_{1/2} = (25.5383 \pm 0.0006) \text{ min}$ ,  $E_{T_{1/2}} = 2.6 \times 10^{-3} \%$ .

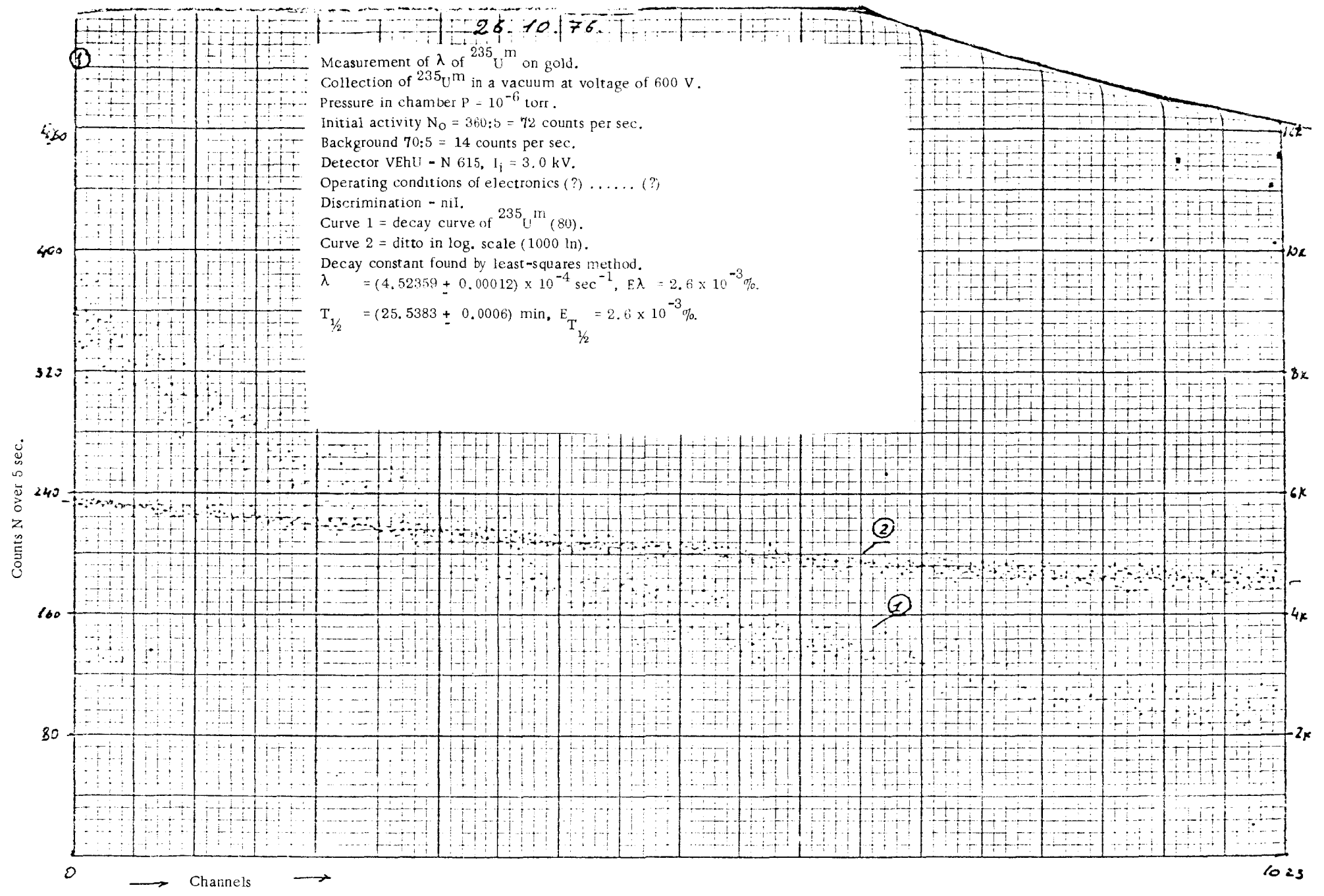


Fig. 3.

- 33 -



Paper presented at the 29th Conference on nuclear spectroscopy  
and the structure of the atomic nucleus (Riga, March 1979)

CONVERSION ELECTRON SPECTRUM OF THE  $(1/2)^+$  ISOMER OF  $^{235}\text{U}$

V.I. Zhudov, A.G. Zelenkov, V.M. Kulakov,  
V.I. Mostovoj, B.V. Odinov

Key words: uranium, isomer, conversion, electron,  
spectrum, transition, energy.

ABSTRACT

The differential conversion electron spectrum of the  $(1/2)^+$  isomer of  $^{235}\text{U}$  was measured. Three lines were detected in the spectrum which correspond to conversion by the  $(6p_{1/2})^2$ ,  $(6p_{3/2})^4$  and 6d electron shells of a uranium atom. The excitation energy of the isomer was determined as  $(76 \pm 2)$  eV.

---

Close to its ground state  $(I_0 \Gamma_0) = (7/2)^-$  a  $^{235}\text{U}$  nucleus has an extremely low-energy isomeric level in terms of nuclear scales  $(I_1 \Gamma_1) = (1/2)^+$  [1, 2]. This level discharges with a half-life  $T_{1/2} \sim 26$  min via an almost completely converted nuclear E3 transition involving the outer electron shells of a uranium atom. The conversion electron spectrum of the  $(1/2)^+$ -isomer of  $^{235}\text{U}$  ( $^{235}\text{U}^m$ ) has been investigated several times [3-6]. However, no clear structure was found in the spectra measured previously. Partly for this reason considerable discrepancies are to be observed in the evaluated excitation energies of  $^{235}\text{U}^m$ . It is assumed that the conversion occurs with the aid of the  $(6p_{1/2})^2$ ,  $(6p_{3/2})^4$  and 6d electron shells of a uranium atom. This assumption is in need of experimental verification, and the excitation energy of the isomer needs to be determined more precisely.

We measured the differential conversion electron spectrum of the  $(1/2)^+$ -isomer of  $^{235}\text{U}$ , identified the electron shells of a uranium atom which participate in the conversion and determined the excitation energy of the isomeric state.

The  $^{235}\text{U}^m$  samples that we investigated were prepared by electrostatic collection of recoil atoms generated during alpha-decay of  $^{235}\text{Pu}$ . The layer of plutonium had a thickness of  $\sim 25 \mu\text{g}/\text{cm}^2$  and was applied by thermal atomization in a vacuum to the inner surface of a platinum hemisphere having a diameter of  $\sim 80 \text{ mm}$ . The collecting electrode - a gold foil covered on one side with a thin layer of uranium tetrafluoride ( $\text{UF}_4$ ) - was located at the centre of the hemisphere. The layer of  $\text{UF}_4$  which was deposited on the gold foil from suspension in dehydrated methyl alcohol served as the base for the preparation of the  $^{235}\text{U}^m$  samples. The collection of recoil atoms was performed in helium at a pressure of  $\sim 0.5 \text{ atm}$  and a negative potential of  $\sim 2 \text{ kV}$  with respect to the potential of the  $^{239}\text{Pu}$  layer. The  $^{235}\text{U}^m$  sources prepared in this way had an effective area of  $1 \times 5 \text{ mm}^2$  and an initial activity of up to  $10^5$  disintegrations per second. Monitoring of the conditions of accumulation and identification of the isomer were performed by means of measurements of its half-life. No  $^{239}\text{Pu}$  impurity was observed in the samples investigated.

The measurements of the differential conversion electron spectrum of  $^{235}\text{U}^m$  were performed on an HP 5950A electron spectrometer [7], the energy range of which (500-1500 eV) was extended by us to 0-2500 eV especially for the purpose of investigating  $^{235}\text{U}^m$ . The basic physical characteristics of the instrument were practically unaffected by the modification. In particular, the energy resolution of the beta spectrometer proper of the ESCA HP 5950A unit remained at  $\sim 0.2 \text{ eV}$  [7]. The energy scale of the instrument was calibrated with an accuracy of  $\sim 0.05 \text{ eV}$  with respect to the X-ray-electron spectra of copper, carbon and gold which have levels with well-known values of the electron binding energy [8]. The binding energy scale of the spectrometer was adjusted to the position of the Fermi level in the X-ray-electron spectrum of palladium.

Measurement was performed in the 0-2500 eV energy range. The conversion lines corresponding to the isomeric transition of  $^{235}\text{U}^m$  were detected below  $\sim 72 \text{ eV}$ . Figure 1 shows in the semi-logarithmic scale the full spectrum of conversion electrons of the isomer collected on a  $\text{UF}_4$  base. This is the result of summation of five separate measurements.

Three conversion lines can be clearly discerned in the  $^{235}\text{U}^m$  spectrum against the background of the intensive tail of the 'zero-energy' electron peak. The nature of these electrons is evidently conditioned by the slowing down of the conversion electrons in the material of the sample and by secondary electron emission. The conversion lines were identified and the

energy of the isomeric transition  $(1/2)^+ \rightarrow (7/2)^-$  of  $^{235}\text{U}$  was determined by comparing the conversion and X-ray electron spectra obtained for the same  $\text{UF}_4$  sample. The regions of the spectra compared in the 50 eV energy window are shown in Fig. 2.

As can be seen from the figure, the conversion lines of  $^{235}\text{U}^m$  correspond to within  $\sim 1$  eV to three X-ray-electron lines of  $\text{UF}_4$ . According to the results of Ref. [9], the first line of the X-ray-electron spectrum of  $\text{UF}_4$  corresponds to the excitation of the  $6p_{1/2}$ -shell of uranium and the 2S-shell of fluorine. The second line is associated with the excitation of the  $6p_{3/2}$ -shell of uranium, and the third includes the excitation of the  $6d7s$ -shell of uranium and the 2p-shell of fluorine. This peak occurs in the wing of the more intensive right-hand peak relating to the excitation of the 5f-electrons of uranium. From the comparison of the spectra it follows that the conversion of the isomeric transition occurs on the  $(6p_{1/2})^2$ ,  $(6p_{3/2})^4$  and 6d electron shells of a uranium atom. Conversion by means of 5f-electrons of uranium was not observed, and participation in the conversion of 7s-electrons is unlikely according to the data in Ref. [10].

The isomeric transition energy was determined from the  $6p_{3/2}$  line of uranium which corresponds to an electron binding energy of  $(19.0 \pm 0.5)$  eV. The energy balance during the excitation of this line in the conversion and photoelectric effect processes may be written as follows:

$$E^* = T_c + E_{\text{bind}} + e\phi \quad (1)$$

$$h\nu = T_{\text{ph}} + E_{\text{bind}} + e\phi \quad (2)$$

where  $E^*$  is the excitation energy of  $^{235}\text{U}^m$ ,  $h\nu$  is the energy of the exciting X-radiation,  $E_{\text{bind}}$  is the electron binding energy of the excited shell,  $e\phi$  is the work function of the spectrometer material, and  $T_c$  and  $T_{\text{ph}}$  are the kinetic energies of conversion electrons and photoelectrons respectively.

From relations (1) and (2) it follows

$$E^* = h\nu + (T_c - T_{\text{ph}}) \quad (3)$$

Use of the spectrum comparison method enables the work function  $e\phi$  to be omitted from the calculations which is advantageous as its precise determination

is quite a complex problem. In our experiments the X-ray-electron spectrum of  $UF_4$  was excited by monochromatized characteristic radiation of aluminium ( $AlK\alpha$ ), the energy of which  $h\nu = 1486.6$  eV. The measured difference ( $T_c - T_{ph}$ ) was  $-1410.7$  eV. Thus the energy of the isomeric transition  $(1/2)^+ \rightarrow (7/2)^-$  of  $^{235}U$  was determined by us to be  $(75.9 \pm 2)$  eV.

In the table our result is compared with the data of other authors.

Table

Data on the energy of the transition  
 $(1/2)^+ \rightarrow (7/2)^-$  of  $^{235}U$

Ref.	Method of measurement	Experimental boundary of the integral conversion spectrum (eV)	Transition energy	Remarks
[3]	Integral conversion electron spectrum	$70.5 \pm 1$	75	Transition energy assumed on the basis of the boundary energy of the integral spectrum
[4]		23	23	
[5]		$30 \pm 2$	$30 \pm 2$	
[6]		$68 \pm 2$	$73 \pm 5$	
Present work	Differential spectrum		$75.9 \pm 2$	Found from $6p_{3/2}$ conversion line of uranium

The authors wish to thank Messrs. A.I. Leonov and V.M. Shatinskij for their assistance with the work, and also D.P. Grechukhin, A.A. Soldatov and Yu.A. Teterin for their useful contributions in the discussion of the results.

REFERENCES

1. F. Asaro and I. Perlman, *Phys. Rev.* 107, 1, 318 (1957).
2. J.R. Huizenga, C.L. Rado, D.W. Engelkemeir, *Phys. Rev.* 107, 1, 319 (1957).
3. M. C. Michel, F. Asaro and I. Perlman, *Bull. Amer. Phys. Soc.*, 2, 18, 394 (1957).
4. M.C. Freedman, F.T. Porter, F. Wagner, I. Day, P. Day, *Phys. Rev.* 108, 3, 836 (1957).

5. N. Mazaki, and S. Shimizu, *Phys. Letters*, 23, №2, 137 (1966)
6. M. Nève de Mèvergnies, *Phys. Letters*, 32B, №6, 482 (1970).
7. M.A. Kelly, C.E. Tyler, *HP-Journal* 2, July 1973.
8. G. Johansson, J. Hedman, et al, *J. Elect. Spectr and Relat. Phenom.* 2.295.1973
9. J.J. Pireaux, N. Martenson, R. Didriksson, K. Siegban  
*Chem. Phys. Letters*, 46, №2, 215 (1977).

[10] GRECHUKHIN, D.P., SOLDATOV, A.A., *Yad. Fiz.* 28 (1978) 1206.

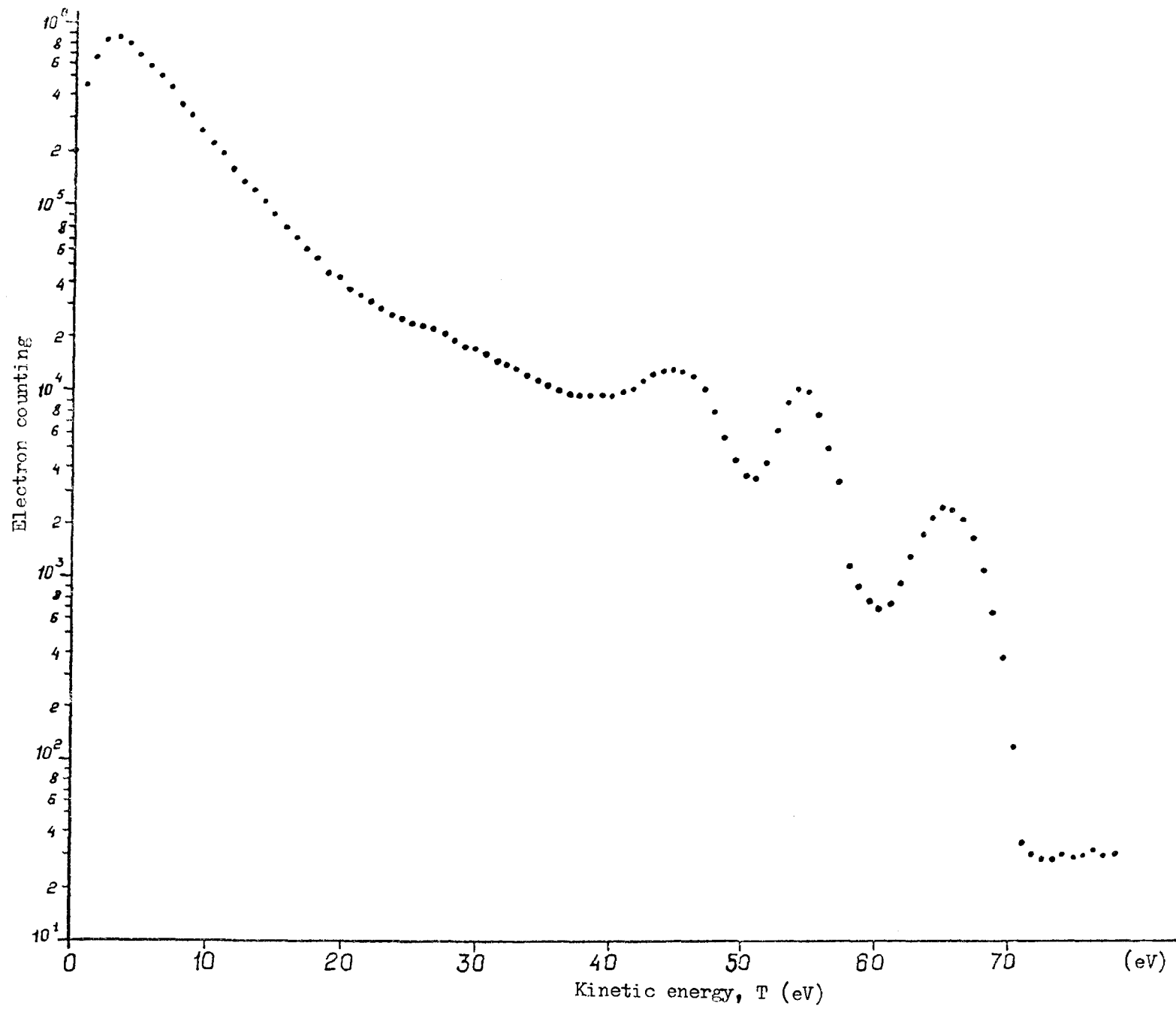


Fig. 1. Conversion electron spectrum of  $^{235}\text{U}$

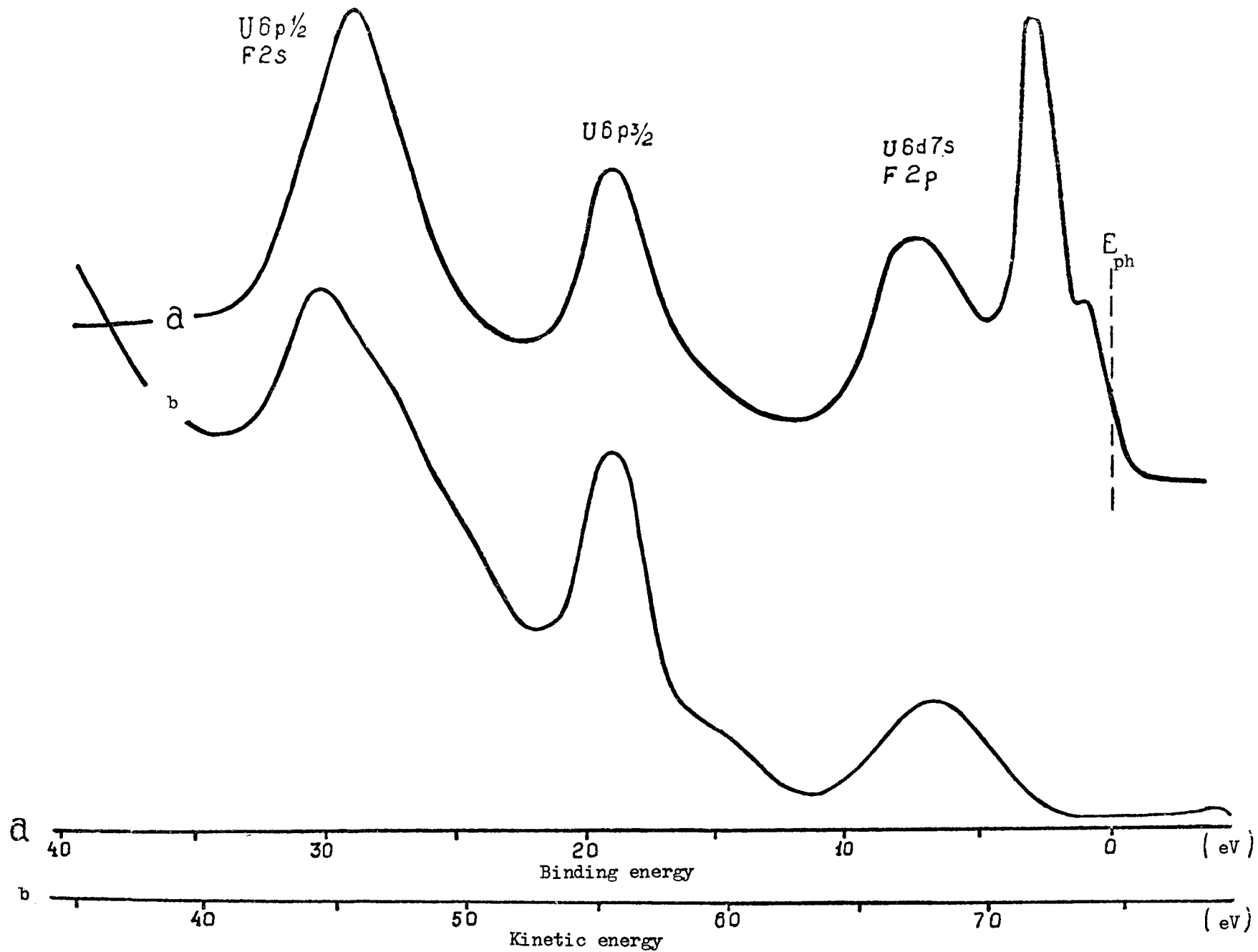


Fig. 2. Comparison of X-ray electron (a) and conversion (b) spectra



COMPARISON OF VARIOUS THEORETICAL MODELS BASED  
ON NEUTRON  $^{242}\text{Pu}$  CROSS SECTION CALCULATIONS

V. A. Konshin

Luikov Heat and Mass Transfer Institute, Minsk, USSR

The previous paper<sup>\*)/1/</sup> submitted to this meeting deals with the energy range of resolved and unresolved resonances (up to 200 keV for  $^{242}\text{Pu}$ ), average statistical parameters, neutron cross section calculations as well as with evaluation of the accuracy of the predictions of neutron cross sections in this energy range. Here we shall therefore analyze the nuclear models for the energy range from 100 keV to 15 MeV.

In the energy range (1 keV - 5 MeV) the compound nucleus mechanism is responsible for the neutron-nucleus interaction. For  $^{242}\text{Pu}$ , in this energy range, only the fission cross section,  $\sigma_f$ , is measured experimentally. Therefore, neutron cross sections ( $\sigma_{n\gamma}$  and  $\sigma_{nn}$ ) can be evaluated only by those theoretical concepts, whose correctness attains special importance.

Neutron cross sections in this energy range have been calculated using Hauser and Feshbach's statistical model allowing for the fission and radiative capture competition for discrete and continuous nucleus-target spectra. With increasing energy of the incoming neutron, the number of reaction channels grows and the width fluctuation factor (S-factor) tends to unity for

---

\*) Reference is made to the Review Paper by V.A. Konshin presented to the Advisory Group Meeting on Transactinium Isotope Nuclear Data, which will be published as part of the Proceedings of that Meeting.

all channels but the one for the compound elastic scattering. As a rule, calculations with the S-factor are made for the energies less than the boundary of discrete and continuous nucleus-target spectra assuming that this factor equals unity for larger energies. For many nuclei, including  $^{242}\text{Pu}$ , the discrete level spectrum, however, is not resolved experimentally at these energies to neglect the effects of width fluctuation and correlation at its boundary (Fig. 1).

Our calculations show that Tepel's approach /2/, applicable in case of many reaction channels with comparable contributions cannot, however, be employed to calculate neutron cross sections for fissile nuclei in the energy range up to 1 MeV. This is attributed to a small number of decay channels and to the strongly competing fission channel available with small  $\nu_f$  (Figs 1 and 2). Meanwhile, the calculations show that already at 1.1 MeV, the neutron cross sections for  $^{242}\text{Pu}$  predicted by Hauser and Feshbach's statistical model with the S-factor and by Tepel's approach coincide for  $\bar{\sigma}_{n\gamma}$  within 10%;  $\bar{\sigma}_{nf}$ , within 10 % and for  $\bar{\sigma}_{nn'}$ , within ~ 2 %. It should be noted that with Tepel's approach used, the sum of the compound reaction cross sections differs from that calculated by the optical model. This difference due to the modified neutron transmission coefficients for the incoming state, however, diminishes with increasing energy and almost vanishes at  $E_n > 1.1$  MeV. Since above 1.1 MeV there are available experimental data for  $\bar{\sigma}_{nf} (^{242}\text{Pu})$ , the fission transmission coefficients,  $T_f$ , can be determined quite accurately and, besides,  $\bar{\sigma}_{n\gamma}$  is much less than other

nonelastic processes, then the sum of elastic and inelastic compound scattering cross sections calculated by Hauser - Feshbach's model and Tepel's formalism proves to be the same. However, as compared to Hauser-Feshbach's model, Tepel's formalism allowing for the correlation of incoming and outgoing elastic channels would more correctly calculate the compound elastic and hence inelastic scattering cross sections for  $^{242}\text{Pu}$  in the energy range between 1.1 MeV and 2.0 MeV. Above 2 MeV, these both formalisms give however the same results. Therefore, at energies above 1.1 MeV, in our calculations Tepel's approach is used instead of Hauser-Feshbach's model. The main difference between these two approaches lies in the expressions for the neutron transmission coefficients for the incoming channel and in the additional term for the elastic scattering cross section:

$$\sigma_{nn'}(E_q) = \frac{\pi}{\kappa^2} \frac{1}{2(2i+1)} \sum_{ejJ} V_{ej}(E) (2J+1) \frac{\sum_{e'j'J'} V_{e'j'J'} (E - \frac{A+1}{A} E_q)}{V_{gJ\pi} + V_{fJ\pi} + \sum_{e''j''q''} V_{e''j''J''} + \alpha(E, J)} \quad (1)$$

$$\alpha(E, J) = \sum_{e'j'i'} \int_{E_{q, \max}}^{\frac{A}{A+1} E} \rho(E', i') V_{e'j'J'} (E - \frac{A+1}{A} E') dE' \quad (2)$$

$$\sigma_{nn', \text{cont}} = \frac{\pi}{\kappa^2} \frac{1}{2(2i+1)} \sum_{ejJ} \frac{V_{ejJ}(E) (2J+1) \alpha(E, J)}{V_{gJ\pi} + V_{fJ\pi} + \sum_{e''j''q''} V_{e''j''J''} + \alpha(E, J)} \quad (3)$$

$$\sigma_{nn'}(E) = \sum_q \sigma_{nn'}(E, E_q) + \sigma_{nn', \text{cont}} \quad (4)$$

$$\sigma_{n\gamma} = \frac{\pi}{\kappa^2} \frac{1}{2(2i+1)} \sum_{ejJ} V_{ejJ} (2J+1) \frac{V_{gJ\pi}}{V_{gJ\pi} + V_{fJ\pi} + V_{nJ\pi}} \quad (5)$$

$$\sigma_{nf} = \frac{\pi}{k^2} \frac{1}{2(2i+1)} \sum_{ejJ} V_{ejJ} (2J+1) \frac{V_{fJ\pi}}{V_{gJ\pi} + V_{fJ\pi} + V_{nJ\pi}} \quad (6)$$

where the modified transmission coefficient,  $V_{ej}$ , for the elastic neutron channel is:

$$V_{ejJ} = T_{ejJ} \left[ 1 + \frac{T_{ejJ}}{\sum_{ej} T_{ejJ}} (W_{ejJ} - 1) \right]^{-1} \quad (7)$$

and  $W_{ejJ}$  is calculated by:

$$W_{ejJ} = 1 + 2 \left[ 1 + \sqrt{T_{ejJ}} \right]^{-1} \quad (8)$$

For other neutron channels as well as for fission and radiative capture channels, the transmission coefficients,  $V_{ejJ}$ , coincide with  $T_{ejJ}$ .

This implies that for a large number of reaction channels with comparable contributions (realized for transactinides at  $E_n > 1.1$  MeV), Tepel's approach allowing for the correlation effects of incoming and outgoing elastic channels seems to give a better approximation.

In the range above the energy of the last resolved level,  $E_{q \max}$ , it is necessary to adopt the concept of the continuous level spectrum. For this purpose the Fermi-gas model is widely used. Of late, the Fermi-gas model has been substantially elaborated to find still wider application. In /3/, a distinct correlation between the level density parameter,  $a$ , and the shell correction,  $\delta W$ , makes it possible to allow for decreasing shell effects in the level density due to excitation energy increase. To this end, the following expression is employed:

$$a(u) = \tilde{a} \left[ 1 + f(u) \frac{\delta W}{u} \right] \quad (9)$$

where  $f(u)=1-\exp(-\gamma u)$  and  $\tilde{a}$  is the asymptotic value of  $a(u)$  at high excitation energies. In /4/,  $\tilde{a}$  has been expressed as:  $\tilde{a} = \alpha A + \beta A^{2/3}$ . For neutron cross section evaluation purposes, we determine  $\tilde{a}$  from  $\langle D (S_n) \rangle_{\text{obs}}$  to take account of the specific features of nuclei.

A point to be is that the effect of the energy dependence of the parameter  $a$  is most substantial for the nuclei near the closed shells. For  $^{242}\text{Pu}$  and transactinides, the shell corrections are relatively small, thus making this effect less pronounced.

The Fermi-gas model is based on complete mixing of the collective degrees of freedom for an excited nucleus and does not, therefore, allow for the collective rotational and vibrational effects. The semi-microscopic level-density approach developed recently by Soloviev et al. /5-7/ enables the allowance for the vibrational and rotational modes. The statistical averaging methods /8-9/ are also widely used to predict level densities although in the adiabatic approach to the collective mode calculations some problems are encountered such as: the difference in collective nucleus motions at various excitation energies, mixing of collective and single-particle modes, etc.

These very problems can be solved by the microscopic methods for direct modelling of the highly excited nucleus state structure /11/. For level density calculations these methods, however, turn to be very tedious and, especially, at higher energies, which hampers their application for nuclear data evaluation.

That is why the statistical method for averaged characteristics of excited nuclei /8-9,12/ is employed to reveal the effect of collective level densities on neutron cross section calculations. Within the framework of this approach, the expression for the level density can be written as:

$$\rho(u, J, \pi) = K_{rot} K_{vibr} \rho_{F-g}(u, J, \pi) \quad (10)$$

where  $\rho_{F-g}(u, J, \pi)$  is defined from the Fermi-gas model;  $K_{rot}$  and  $K_{vibr}$  are the coefficients for level density increase due to rotational and vibrational modes. In /4/, /9/, /12/ the simple expressions are obtained for  $K_{rot}$  and  $K_{vibr}$  :

$$K_{rot} = F_{\perp} t = F_{\perp} \sqrt{\frac{u}{a}} \quad (11)$$

$$K_{vibr} = \exp [0,25 u^{2/3}] \quad (12)$$

where  $F_{\perp}$  is the inertia moment of the deformed nucleus relative to the axis normal to the symmetry axis ( $F_{\perp} = 0.4 mAR_0^2 \cdot (1 + \frac{1}{3}\beta)$ ).

As compared to the traditional expression from the Fermi-gas model, a sufficiently large factor incorporated into (10) gives a considerable decrease in the parameter  $a$ .

At present, the superfluid nucleus model calls a great deal of attention in nucleus level density calculations because it enables to correctly allow for residual correlation interactions. A simple version of this model is proposed in /8/. The difference between the superfluid nucleus and Fermi-gas models consists in determining  $\sigma^2$  and  $\rho(u)$  in such a way:

$$\rho(u) = \frac{\exp[\mathcal{S}(\beta, \alpha_z, \alpha_N)]}{(2\pi)^{3/2} |\text{Det}(\beta, \alpha_z, \alpha_N)|^{1/2}} \quad (13)$$

where  $\beta$  is the reversal of the thermodynamic temperature  $t$ ,  $\alpha_{z,N} = \lambda_{z,N} \beta$  ( $\lambda_{z,N}$  are chemical potentials for proton and neutron components) and  $\text{Det}(\beta, \alpha_z, \alpha_N)$  is the determinant of the second entropy derivatives. Following /8/, the quantities, necessary to determine the level density by the superfluid nucleus model, can be defined as:

$$\mathcal{S} = 2\alpha \frac{t_c^2}{t} [1 - f^2(t)] \quad (14)$$

$$\sigma^2 = \frac{6\alpha}{\pi^2} \langle m^2 \rangle t_c [1 - f^2(t)] \quad (15)$$

$$\mathcal{U} = E + S_n = \frac{3}{2} \alpha t_c^2 [1 - f^2(t)] = \mathcal{U}_c [1 - f^2(t)] \quad (16)$$

$$\text{Det} = \frac{18\alpha^3 t_c^5}{\pi^4} [1 + f^2(t)]^2 [1 - f^2(t)] \quad (17)$$

where  $f(t)$  satisfies:

$$f(t) = \text{th} \left[ \frac{t_c}{t} f(t) \right] \quad (18)$$

The quantity  $t_c$  in equations (14) through (17) is the critical temperature which in this model is associated with the correlation function for the ground state  $\Delta_0$  as  $t_c = \frac{\Delta_0}{2}$ .

Above the phase transition,  $t_c$ , the function  $f(t)=0$  and we obtain the Fermi-gas model expressions where the excitation energy is related to the temperature in terms of :

$$\mathcal{U} = \alpha t^2 + \frac{1}{8} \alpha \Delta_0^2 \quad (19)$$

It should be noted that in this version of the above mo-

del, the values of the energy shift,  $E_{cond}$ , and phase transition,  $t_c$ , are smaller than those in the approximation for the constant matrix element of pair interaction ( $E_{cond} = \frac{3\alpha}{2\pi^2} \Delta_o^2$ ,  $t_c = 0.567 \Delta_o$ ). This may considerably change the level density.

The above approach holds for even-even nuclei. However, as is shown in /13/, the relations for the superfluid nucleus model are also valid for odd and odd-odd nuclei if the excitation energy is defined as:

$$U = U_{\text{even-even}} + \begin{cases} \Delta_o & \text{for odd nuclei} \\ 2\Delta_o & \text{for odd-odd nuclei} \end{cases}$$

The value of  $\Delta_o$  may be found from  $\Delta_o = 12.5 \cdot A^{-1/2}$  MeV /4/. In the higher energy range, the correlation functions for the ground state of proton and neutron components

$$\Delta_{oZ} = \Delta_{oN} = \Delta_o.$$

This version of the superfluid nucleus model allowing for the collective modes is employed to calculate neutron cross sections. A contribution of the rotational and vibrational modes to the level density is determined by introducing factors (11) and (12) into formula (13).

The above level density models give different energy-dependent level densities, which affects the cross sections calculated by the statistical model. For the excitation energy,  $U$ , equal to the neutron binding energy, the level density is almost the same in all models. The level densities calculated by the generally accepted Fermi-gas model, the Fermi-gas model both involving the collective effects of rotational and vibrational modes and the superfluid nucleus model slightly differ at  $U > S_n$ . At  $U < S_n$ , however, the level densities strongly differ in all models and greatly differ -

ing level densities should therefore most strongly affect the calculations of the cascade  $\gamma$ -ray emission (yield and  $\gamma$ -ray production cross section) as well as inelastically scattered neutron spectrum.

For  $^{242}\text{Pu}$ ,  $^{243}\text{Pu}$ ,  $^{238}\text{U}$  and  $^{239}\text{U}$ , the values of the level density parameter  $a$  with a norm to  $\langle D \rangle_{\text{obs}}$  are obtained using the above models and given in Table 1.

Table 1

Values of the parameter  $a$  for various level density models

Calculation model	$a, \text{ MeV}^{-1}$			
	$^{238}\text{U}$	$^{239}\text{U}$	$^{242}\text{Pu}$	$^{243}\text{Pu}$
Fermi-gas model	31.09	33.26	29.13	31.81
Fermi-gas model involving collective modes	19.10	20.07	17.74	19.25
Fermi-gas model involving energy dependence $a(u)$ (the $\tilde{a}$ -value is given in the table)	33.28	35.59	31.83	35.00
Fermi-gas model involving collective effects and $a(u)$	20.35	21.37	19.26	21.04
Superfluid nucleus model	52.02	59.68	45.31	57.05
Superfluid nucleus model involving collective effects	21.63	21.10	19.20	20.05

Table 1 shows that an account of the energy dependence  $a(E)$  for transactinides does not almost alter the  $a$ -parameter. The enormously large value of  $a$  is observed when the above version of the superfluid nucleus model is used, with neglect of

the collective effects (probably, at  $U=S_n$  decreasing entropy is compensated by a sharp increase in the  $a$ -parameter). The account of the collective effects sharply decreases this parameter, and in both models they become similar to each other and to the quasiclassical value ( $a=0.075 A$ , for  $^{243}\text{Pu}$   $a=18.22 \text{ MeV}^{-1}$ ). The effect of different models for nuclear level density on neutron cross section calculations can be most vividly demonstrated by  $\sigma_{ny}$  predictions.

The energy dependence of the available experimental data for  $\sigma_f(^{242}\text{Pu})$  from 0.2 to 1 MeV points to a sharp increase in fission penetrability. This means that only the continuous spectrum of fission transition states can be used in this energy range. The total fission penetrability for the compound nucleus state,  $J^\pi$ , at the excitation energy  $E_n+B_n$  can therefore be represented as:

$$T_f^{J^\pi}(E_n) = \int_0^\infty \frac{1}{1 + \exp\left[-\frac{2\pi(E_n - V_F - \varepsilon)}{\hbar\omega_F}\right]} \rho_f(\varepsilon, J^\pi) d\varepsilon \quad (20)$$

where

$$\rho_f(\varepsilon, J^\pi) = C_F (2J+1) \exp\left[-\frac{(J+1/2)^2}{2\sigma^2}\right] \exp\left(\frac{\varepsilon}{\theta_f}\right)$$

is the density of the transition states from the constant temperature level density model /14/, with energy exceeding the fission threshold by  $\varepsilon$ . The transition state density parameters are determined from the agreement between the predicted and experimental  $\sigma_f$  from 0.2 to 1.1 MeV and prove to be  $C_F=0.5$ ;  $\theta_F=0.3$ ;  $\sigma=5.7$ ;  $V_F=0.5 \text{ MeV}$  (taken from the boundary of the neutron binding energy);  $\hbar\omega_F=0.5 \text{ MeV}$ . The comparison of the parameterized and experimental fission cross sections from 0.2 to 1.1 MeV is shown in Fig. 2.

The discrepancy between calculated and experimental  $\sigma_f$  does not exceed 10% in the whole range.

Since in the energy range from 0.2 MeV to 5.0 MeV a unique set of the parameters fails to govern well the values of  $\sigma_f$  and the experimental fission cross section is comparatively accurate, the fission competition with inelastic scattering and radiative capture processes from 1.1 MeV to 5 MeV is allowed for by the fission transmission coefficients:

$$T_F^{J\pi} = (2J+1) \exp\left[-\frac{(J+1/2)^2}{2\sigma^2}\right] T_f(E) \quad (21)$$

where  $T_f(E)$  is found by fitting the calculated and experimental values of  $\sigma_f$ .

As the calculated values of  $\sigma_f$  ( $^{242}\text{Pu}$ ) are fitted to their experimental values, the radiative capture cross section,  $\sigma_{n\gamma}$ , turns to be mostly sensitive to the choice of one or another level density model. This choice can be made uniquely only with the available experimental data for  $\sigma_{n\gamma}$  in a wide energy range. Therefore, calculations are also made for  $\sigma_{n\gamma}$  ( $^{238}\text{U}$ ).

The radiative capture transmission coefficients are calculated, as is usually done to the dipole transition approximation, with the competition of  $(n, \gamma n')$  and  $(n, \gamma f)$  reactions being allowed for:

$$T_{\gamma J\pi}(E^*) = 2\pi \int_{\frac{A}{A+1}E_n}^{E^*} \sum_{J_k=|J-1|}^{J+1} \rho(E^* - \varepsilon_\gamma, J_k \pi_k) f(E^*, \varepsilon_\gamma) \frac{T_{\gamma J_k \pi_k}(E^* - \varepsilon_\gamma) d\varepsilon_\gamma}{T_{\gamma J_k \pi_k} + T_f^{J_k \pi_k}} \quad (22)$$

where  $E^*$  is the excitation energy of the compound nucleus;  $\varepsilon_\gamma$  - the energy of the emitted  $\gamma$ -quantum;  $f(E^*, \varepsilon_\gamma)$  - the spectral factor;  $\rho(E^* - \varepsilon_\gamma, J_k \pi_k)$  the compound nucleus level density

at the excitation energy upon the  $\gamma$ -ray emission.

Strictly speaking, the expression for total radiative penetrability should incorporate two terms, one for integrating for the continuous and another for summing up the discrete compound-nucleus level spectra. However, the uncertainty associated with approximating the discrete level spectrum band by the continuous one proves to be very small. The problem of magnetic dipole transition intensity for heavy nuclei is not yet clear. But with the discrete spectrum for transition states of the fissile nuclei approximated, the account of only electric dipole transitions does not affect  $\sigma_{n\gamma}$  calculations.

$\sigma_{n\gamma}$  is usually calculated by the Weisskopf spectral factor /15/:

$$f(E^*, \epsilon_\gamma) = C_W \epsilon_\gamma^3 \quad (23)$$

and by the Lorentz spectral factor for deformed nuclei /16/:

$$f(E^*, \epsilon_\gamma) = C_L \frac{8}{3} \frac{NZ}{A} \frac{e^2}{\hbar c} \frac{1.4}{m_e c^2} \sum_{i=1}^2 \frac{i}{3} \frac{\Gamma_{G_i} \epsilon_\gamma^4}{(\epsilon_\gamma^2 - E_{G_i}^2)^2 + (\Gamma_{G_i} \epsilon_\gamma)^2} \quad (24)$$

with the giant resonance parameters for transactinides /14/:  $E_{G_1} = 11$  MeV,  $E_{G_2} = 14$  MeV,  $\Gamma_{G_1} = 2.9$  MeV,  $\Gamma_{G_2} = 4.5$  MeV.

Several authors /17/ show preference to the Weisskopf spectral factor over the Lorentz one because the  $\sigma_{n\gamma}$  values calculated with the Lorentz factor are essentially higher than the experimental data. However, the spectral factor in the Lorentzian form gives a better agreement between the theoretical and experimental data for the  $(n, \gamma f)$ -

process width for strongly fissile nuclei. Since expression (22) for radiative capture penetrability contains the spectral factor as well as the compound nucleus level density, the discrepancy between theory and experiment may presumably be attributed to the incorrect level density model used. In /18/, it is shown that the allowance for the collective effects in the nucleus level density can improve the agreement between the experimental data for  $\sigma_{n\gamma}$  and those calculated with the Lorentz spectral factor. In /18/, the calculations are made for  $^{238}\text{U}$  only up to 1 MeV with neglect of the fission competition. To choose a proper theoretical model for  $\sigma_{n\gamma}$  calculations for  $^{242}\text{Pu}$  and other transactinides, we have calculated  $\sigma_{n\gamma} (^{238}\text{U})$  from 0.1 to 3.0 MeV (with the fission competition being taken into account) using various models for the nuclear level density, both spectral factors and with allowance for the uncertainties in  $\langle \Gamma_\gamma \rangle / \langle D \rangle$  and in neutron transmission coefficients.

Figure 3 shows the comparison between the experimental and calculated radiative capture cross section  $\sigma_{n\gamma} (^{238}\text{U})$  in the energy range from 0.1 to 3.0 MeV.

First of all, consider the effect of the uncertainties in  $\langle \Gamma_\gamma \rangle$  and  $\langle D \rangle$  on  $\sigma_{n\gamma}$  calculations.

In Fig. 3, curves 1-7 are calculated with the parameters:  $\langle D \rangle_{\text{obs}} = (17.7 \pm 0.7) \text{ eV}$  /19/ and  $\langle \Gamma_\gamma \rangle = 23.5 \text{ meV}$ . This value of  $\langle \Gamma_\gamma \rangle$  agrees with Abagyan's estimate /20/ within 3 %. The uncertainty associated with choosing  $\langle \Gamma_\gamma \rangle$ , approximately equal to 5 %, leads to the same error  $\sigma_{n\gamma}$  calculated in the same energy range. The error in  $\langle D \rangle_{\text{obs}}$  yields the substantial uncertainty in calculated  $\sigma_{n\gamma}$ .

So the value of  $\langle D \rangle_{\text{obs}} = (17.7 \pm 0.7) \text{ eV}$  /19/ is apparently based on Carraro's results /21/ who obtained  $\langle D \rangle_{\text{obs}}$  analysing the resonances at the energies up to 2 keV and assuming all these resonances to be s-levels. Recent measurements lead to higher values of  $\langle D \rangle_{\text{obs}}$  (e. g.  $\langle D \rangle_{\text{obs}} = 20.8 \pm 0.3 \text{ eV}$  /20/) which are in good agreement with the evaluated data /20/ ( $\langle D \rangle_{\text{obs}} = 20.8 \text{ eV}$ ). As is seen, Carraro's data for  $\langle D \rangle_{\text{obs}}$  /21/ and those in /22/ do not coincide within the errors mentioned by the authors. Calculations show that the discrepancy in  $\sigma_{n\gamma}$  caused by these two extreme values of  $\langle D \rangle_{\text{obs}}$  is considerable and amounts to  $\sim 15\%$  at 1 MeV (Fig. 4). In Fig. 4, curve 3 is constructed at  $\langle D \rangle_{\text{obs}} = 17.7 \text{ eV}$  using the Fermi-gas level density model involving the collective effects and the Lorentz spectral factor: curve 8 is plotted employing the same model at  $\langle D \rangle_{\text{obs}} = 20.8 \text{ eV}$ . All curves 1 through 7 (Fig. 3) should be normalized, if necessary, to  $\langle D \rangle_{\text{obs}} = 20.8 \text{ eV}$ .

It should be noted that the  $\sigma_{n\gamma}$  curves in Figs 3 and 4 are calculated by the statistical model with the neutron transmission coefficients estimated from the spherical optical model. This is because our computer programs for cross section calculations by the coupled channel method are not yet combined with the computer program realizing the statistical model. Therefore,  $\sigma_{n\gamma}$  is renormalized by the compound-nucleus formation cross section,  $\sigma_c$ , determined from the spherical and non-spherical optical models. This renormalization gives a  $\sim 5-10\%$  decrease in  $\sigma_{n\gamma}(^{238}\text{U})$ . Final conclusions on the  $\sigma_{n\gamma}$  cross sections affected by the neutron transmission coefficients calculated with the

deformed potential will be made later.

This analysis manifests that the generally accepted Fermi-gas model gives a considerable discrepancy between the calculated and experimental  $\sigma_{n\gamma}$  cross sections for both spectral factors (Fig. 3), which cannot be explained by the uncertainty in the parameters used. A better agreement between the calculated and experimental  $\sigma_{n\gamma}$  cross sections is attained from the Fermi-gas and superfluid nucleus models both involving the collective modes. The energy dependence of the  $a$ -parameter when allowed for slightly contributes to the calculated radiative capture cross section in this energy range. So at 3 MeV, this contribution is no more than 4 %, while  $\sigma_{n\gamma}$  cross sections calculated by various level density models differ several times.

The use of the Lorentz spectral factor seems to be more substantiated as it gives correct radiative strength functions and experimental data for  $(n, \gamma_f)$ -widths.

The  $\sigma_{n\gamma}$  curve plotted according to the superfluid nucleus model and the Lorentz spectral factor better fits the experimental data than with the Fermi-gas model for the collective modes and the Lorentz spectral factor. Some uncertainty in the parameters of the used version of the superfluid nucleus model (in particular, phase transition energy) rejects, however, the conclusion on the validity of the relationship between these two curves for other nuclei. The  $\sigma_{n\gamma}$  ( $^{242}\text{Pu}$ ) calculations (Fig. 5) show that for this nucleus the above curves exchange their positions, i. e. the radiative capture cross section calculated by the superfluid nucleus model with the collective modes turns to be larger than

that determined by the Fermi-gas model also taking into account the collective modes. Note that the superfluid nucleus model possesses one more specific feature: the use of the Weisskopf spectral factor gives larger  $\sigma_{n\gamma}$  cross sections than of the Lorentz spectral factor. The situation is quite reverse, for the Fermi-gas model. This case should be studied more thoroughly in future.

Therefore, the  $\sigma_{n\gamma}$  cross sections for  $^{242}\text{Pu}$  are evaluated from the results obtained by the Fermi-gas model that allows for the collective modes and the Lorentz spectral factor. For  $^{242}\text{Pu}$ , the radiative widths are normalized to  $\langle \Gamma_{\gamma} \rangle_{\text{obs}} = 22.6$  meV. The normalization constants are :  $C_W = 4.788 \cdot 10^{-8}$ ,  $C_L = 0.819$  when the Fermi-gas model is used with no regard for the collective modes;  $C_W = 2.79 \cdot 10^{-8}$  and  $C_L = 0.415$  when the Fermi-gas model is adopted with regard for the collective modes;  $C_W = 9.115 \cdot 10^{-8}$  and  $C_L = 1.284$  when the superfluid nucleus model is employed with regard for the collective modes.

Figure 5 presents  $\sigma_{n\gamma}(^{242}\text{Pu})$  cross sections calculated by various level density models. Note that for the energy range from the boundary of discrete and continuous nucleus-target level spectra (1.15 MeV) to 2 MeV, the underestimated level density of the residual nucleus results in somewhat overestimated values of  $\sigma_{n\gamma}$ . This is especially true for the traditional Fermi-gas model.

With the experimental  $\sigma_f$  data available and due to a small value of  $\sigma_{n\gamma}$  in this energy range, it is the correctness of the neutron transmission coefficients contributing primarily to the compound nucleus formation cross section

that provides the reliable calculation of the inelastic scattering cross section. For deformed nuclei ( $^{242}\text{Pu}$ ) the neutron transmission coefficients are best of all calculated by the coupled channel method with non-spherical potential parameters fitted to the input experimental data. The uncertainties in the neutron cross sections calculated by the statistical model are associated with the use of the spherical optical potential and can be, to a considerable extent, compensated by normalization to the compound nucleus formation cross section estimated by the coupled channel method.

If  $\bar{\sigma}_f$  is fitted to the experimental data, then the choice of the level density model does not practically affect the value of the inelastic scattering cross section. Different nucleus-target level densities in different models causes both a variation of the discrete-to-continuous level spectrum ratio for inelastic scattering cross sections and a change of discrete level excitation cross sections (Fig.6). This implies that the choice of the level density model greatly influences the scattered neutron spectrum. Indeed, the experimental data for neutron spectra give smaller values of the  $a$ -parameter against the Fermi-gas model. This is one more evidence of the incorrectness of the traditional Fermi-gas model and the necessity of using other level density models that fairly fit all types of the experimental data.

In our work the coupled channel method is applied to evaluate neutron cross sections for transactinides. This method is known to allow calculation of  $\bar{\sigma}_t$ ,  $\bar{\sigma}_r$ ,  $S_0$ ,  $S_1$ ,  $\bar{\sigma}_{\text{shape-el}}$ , angular distributions of elastically and in-

elastically scattered neutrons and direct excitation cross sections for the first levels of the main rotational band. To find the potential parameters, only experimental data for the strength functions  $S_0$ ,  $S_1$ ,  $\bar{\sigma}_t$  at energies from 10 keV to 15 MeV can be directly used. Experimental results for first-level excitation and elastic scattering cross sections may be adopted only above 3 MeV, when the compound contribution to the first-level excitation cross section is negligible, as compared to direct excitation. The data for the angular distributions of elastically scattered neutrons cannot be generally used to achieve the optimum potential parameters because this method is sensitive to the distributions at larger angles that usually possess the isotropic part caused either by the compound contribution at low energies or by the unresolved low level contribution at high energies. In the majority of cases, it is therefore only possible to compare the calculated and experimental elastically scattered neutron angular distributions rather than to use them for potential parameter determination.

Our computer program realizing the coupled channel method is combined with the automatic search program for potential parameters that is the best fit of the experimental data. Since this problem requires a great deal of the computer time, many efforts are made to speed up the counting.

In principle, it is possible to simultaneously and automatically fit all potential parameters when the experimental data adequate to this model are taken into account. However, this search for the potential parameters is not optimum as

far as the computer time is considered. Calculations show that a two-step search is more advisable. First, the SPTR-method proposed by Largange /23/ is used. This implies that the potential parameters, including the deformation ones, are determined from the strength functions  $S_0$ ,  $S_1$  and the potential scattering radius, while the energy dependences of the imaginary and real parts of the potential are found from the energy dependence  $\sigma_t$ . The preliminary parameters are then more accurately defined by searching for the parameters that minimize the total value of  $\chi^2$ , using all necessary experimental data. This approach allows one order and more shorter computer time required to search for the optimum potential parameters.

As an example, consider the first version of the potential parameters obtained for  $^{238}\text{U}$ . The following data are used:  $S_0 = (1.0 \pm 0.1) \cdot 10^{-4}$ ,  $S_1 = (1.92 \pm 0.3) \cdot 10^{-4}$ ,  $\sigma_t$  from 50 keV to 15 MeV.

At the second step of fitting, apart from these data, use is made of the results /24/ for angular distributions of elastically scattered neutrons as well as for inelastically scattered neutrons at the levels  $2^+$ ,  $4^+$  for 2.5 and 3.4 MeV. A contradiction appears to exist between a high value of the total cross section  $\sigma_t$  at 3.4 MeV and a comparatively low value of the differential elastic scattering cross section at small angles /24/.

The fitting gives the following preliminary values of the potential parameters for  $^{238}\text{U}$ :

$$V_R = 47.5 - 0.3 E_n, \quad a_R = 0.62 \text{ f}, \quad R_R = 7.644092 \text{ f} \quad (r_{OR} = 1.233485 \text{ f})$$
$$W_D = 2.7 + 0.4 E_n, \quad a_D = 0.58 \text{ f}, \quad R_D = 7.808408 \text{ f} \quad (r_{OD} = 1.259999 \text{ f})$$

$$V_{S0}=7.5 \text{ MeV}, \quad a_{S0}=0.62 \text{ f}, \quad R_{S0}=7.644092 \text{ f} \quad (r_{S0}=1.233485 \text{ f}) \\ \beta_2 = 0.216, \quad \beta_4 = 0.067.$$

The parameters of this potential differ from the first version of Lagrange's potential /23/ by somewhat different radius of the real potential part. The strength functions calculated by the above potential parameters are equal to :  
 $S_0 = 1.06 \cdot 10^{-4} \text{ (eV)}^{-1/2}$ ,  $S_1 = 2.16 \cdot 10^{-4} \text{ (eV)}^{-1/2}$ ,  $R = 9.23 \text{ f}$ .  
This value of  $S_0$  seems to be somewhat overestimated ( $\sim 10\%$ ).  
At present we are evaluating this quantity more carefully using the data for the resolved resonance energy range and  $\sigma_t$  results in the keV range. Preliminarily,  $S_0$  proves to be  $0.94 - 0.96 \cdot 10^{-4} \text{ eV}^{-2}$  and is used to obtain the deformed potential parameters for  $^{238}\text{U}$ .

Figure 7 presents the results for the direct part of the differential neutron scattering cross sections calculated with the above potential parameters at three low levels of the rotational band for  $^{238}\text{U}$  at 3.4 MeV.

The uncertainty in the  $\beta_{20}$  parameter for  $^{238}\text{U}$  determined as a difference in two potential fittings made for the same experimental data equals 8%. Within this uncertainty, the  $\beta_{20}$  parameter is the same for  $^{238}\text{U}$  and  $^{242}\text{Pu}$ . The calculations of neutron cross sections for  $^{242}\text{Pu}$  with  $\beta_{20} = 0.228$  and the above potential parameters (with a small correction for the isotropic effect and nucleus radius) show that  $S_0$  is too high, and therefore the  $\beta_{20}$  parameters are taken the same for  $^{238}\text{U}$  and  $^{242}\text{Pu}$ .

Further development of the coupled channel method for nuclear data evaluation purposes should imply: more accurate

knowledge of the deformation parameters not only from the theory and experiment on neutron scattering but also from other sources ( e. g. using the Nilsson model or the Harti-Fok method as well as spectroscopic experimental data) ; account of more complicated collectives states than pure vibrational or rotational levels; more detailed study of the channel coupling for odd nucleus-targets in terms of the nuclear structure; more thorough investigation of the role of the isospin potential for actinides and proton scattering; experiments may shed some light on this problem.

#### R E F E R E N C E S

- 1 Konshin, V. A., Evaluation and Calculation of Neutron Transactinide Cross Sections, Report to Secondary Advisory Group Meeting on Transactinium Isotope Nuclear Data, CEN Cadarache, France, April 30-May 5, 1979.
- 2 Tepel, J. W. , et al., Phys. Letters, 1974, v. 49B, p. 1.
- 3 Ignatyuk, A. V., Smirenkin, G. N., and Tishin, A. G., Yadernaya Physika, 1975, v. 23, p. 485.
- 4 Ignatyuk, A. V., Istekov, K. K., and Smirenkin, G. N., Proc. 4th All-Union Conference on Neutron Physics, Kiev, 1977, pt. 1, p. 60.
- 5 Soloviev, V. G., Stoyanov, Ch., and Vdovin, A. I., Nucl. Phys. , 1974, v. A224, p. 411.
6. Soloviev, V. G. and Malov, L. A., Nucle. Phys., 1972, v. A196, p. 433.

- 7 Voronov, V. V., Komov, A. L., Malov, L. A., and Soloviev, V. G., Nuclear Physics, 1976, v. 24, p. 504, (Sov.J.)
- 8 Ignatyuk, A. V. and Shubin, Yu. N., Izv. AN SSSR, Ser. Fiz., 1975, v. 37, p. 1947.
- 9 Ignatyuk, A. V., Proc. of the Meeting on the Use of Nuclear Theory in Neutron Data Evaluation, Triest, IAEA, 1976, v. 1, p. 211.
- 10 Dossing, T. and Jensen, A. S., Nucl. Phys., 1974, v. A222, p. 493.
- 11 Soloviev, V. G., Proc. of the Intern. Conf. on Interactions of Neutrons with Nuclei, Lowell, USA, 1976, v. 1, p. 421.
- 12 Blokhin, A. I., Ignatyuk, A. V., and Sokolov, Yu. V., Proc. 3rd All-Union Conference on Neutron Physics, Kiev, 1975, pt. 3, p. 8.
- 13 Ignatyuk, A. V. and Sokolov, Yu. V., Proc. 2nd All-Union Conference on Neutron Physics, Kiev, 1976, pt. 2, p. 32.
- 14 Lynn, J. E., AERE-R-7468, 1974.
- 15 Blatt, J. and Weisskopf W., Theoretical Nuclear Physics, Izd. IL, Moscow, 1954.
- 16 Veysiére A., Beil, H., Bergere, R., Carlos, P., and Lepretre, A., Nucl. Phys., 1973, v. A199, p. 45.
- 17 Fricke, M. P., Lopez, W. M., Friesenhahn, S. J, Carlson, A. D., and Costello, D. G., Proc. of the Intern. Conf. on Nuclear Data for Reactors, Helsinki, 1970, v. 2, p. 281.
- 18 Blokhin, A. I., Ignatyuk A. V., Platonov, V. P. and Tolstikov, V. A., Nuclear Constants, 1976, vyp. 21, p. 3.

- 19 Mughabghab, S. F. and Garber, D. I., BNL-325, 3rd Ed., 1973, v. 1.
- 20 Abagyan, L. P., Korchagina, Zh. A., Nikolaev, M. N., and Nesterova, K. I., Nuclear Constants, 1972, vyp. 8, pt. 1, p. 121.
- 21 Carraro G. and Kolar W., Proc. of the Internat. Conference on Nuclear Data for Reactors, Helsinki, 1970, v. 1, p. 403.
- 22 Rahn, F. J., et al., Phys. Rev., 1972, v. 6, p. 1854.
- 23 Lagrange, Ch., Proc. of the EANDC Topical Discussion on "Critique of Nuclear Models and Their Validity in the Evaluation of Nuclear Data", NEANDC(J)38L, 1975, p. 58.
- 24 HaoUat G., Sigaud, J., Lanchkar, J., Lagrange, Ch., Duchemin, B., and Patin, Y., NEANDC(E)180L and NEANDC(E)196L, 1978.

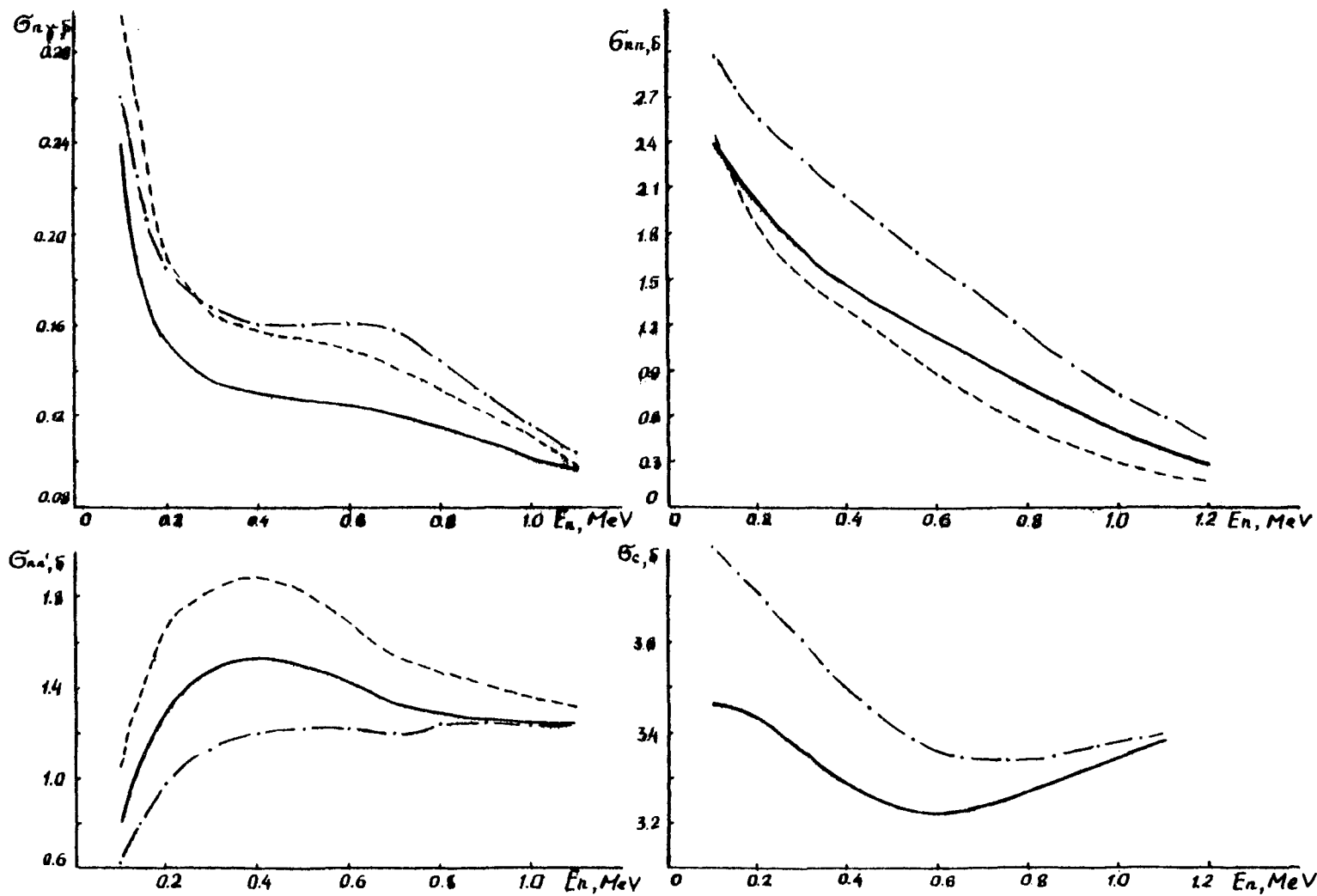


Fig. 1 Comparison of different approaches to calculation of radiative capture, elastic scattering, inelastic scattering and compound-nucleus formation cross sections for  $^{242}\text{Pu}$  (level density Fermi-gas model with collective modes, Lorentz spectral factor): —, Tepel's formalism, ---- Hauser-Feshbach's formalism with no regard for the S-factor; - · - ·, Hauser-Feshbach's formalism with regard for the S-factor.

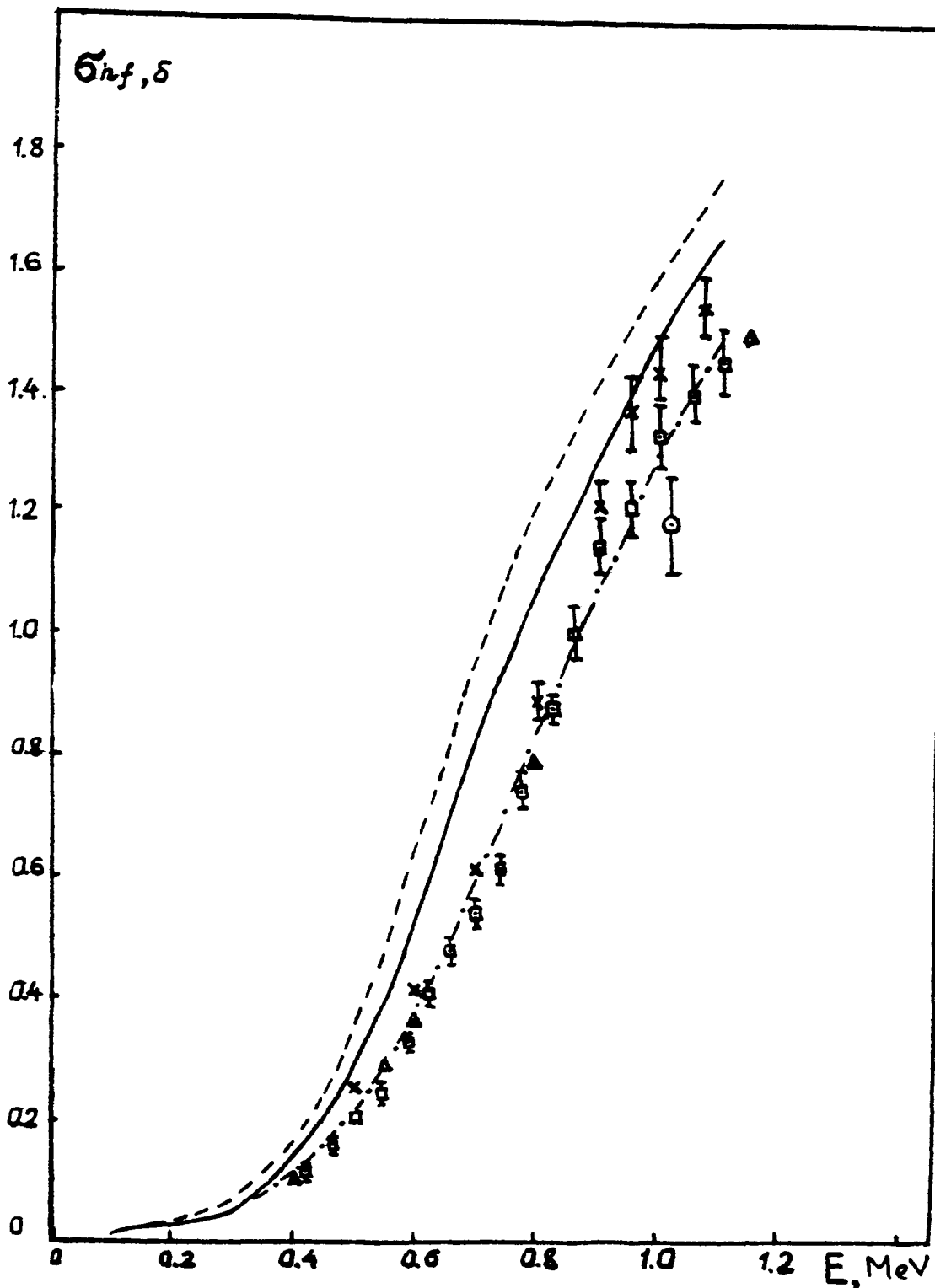


Fig. 2 Comparison of the experimental and predicted values of  $\sigma_{nf}(^{242}\text{Pu})$  (—, Tepel's formalism; ----, Hauser-Feshbach's formalism with no regard for the S-factor; - · - · -, Hauser-Feshbach's formalism with regard for the S-factor).

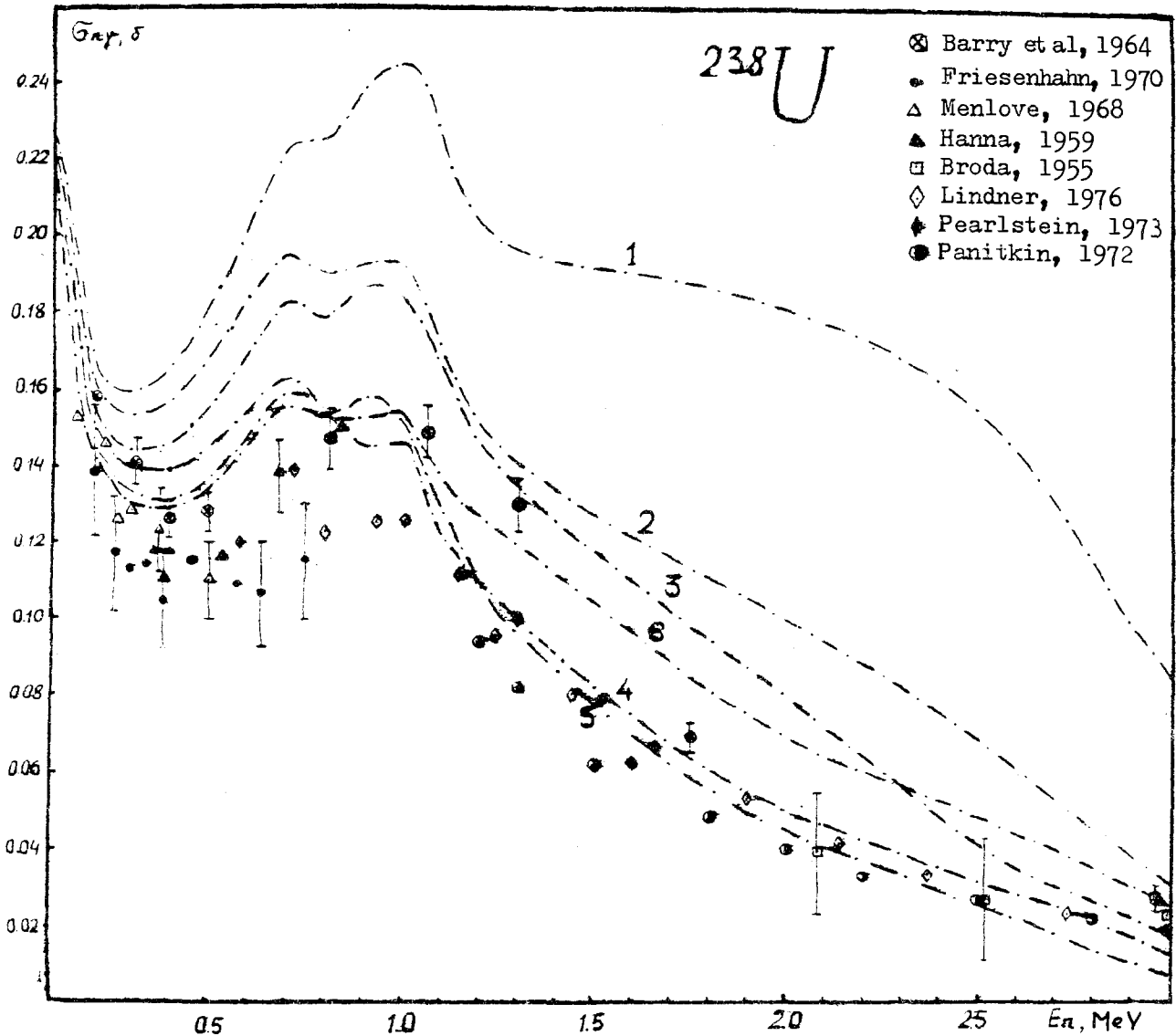


Fig. 3 Comparison of the experimental and predicted data for  $\sigma_{n\gamma}(^{238}\text{U})$  (curve 1, level density Fermi-gas model, Lorentz spectral factor; 2, Fermi-gas model and Weisskopf factor; 3, Fermi-gas model with collective modes, Lorentz factor; 5, the same as for curve 3 but with Weisskopf factor; 4, superfluid nucleus model with collective modes, Weisskopf factor; 6, the same as for curve 4 but with Lorentz factor).

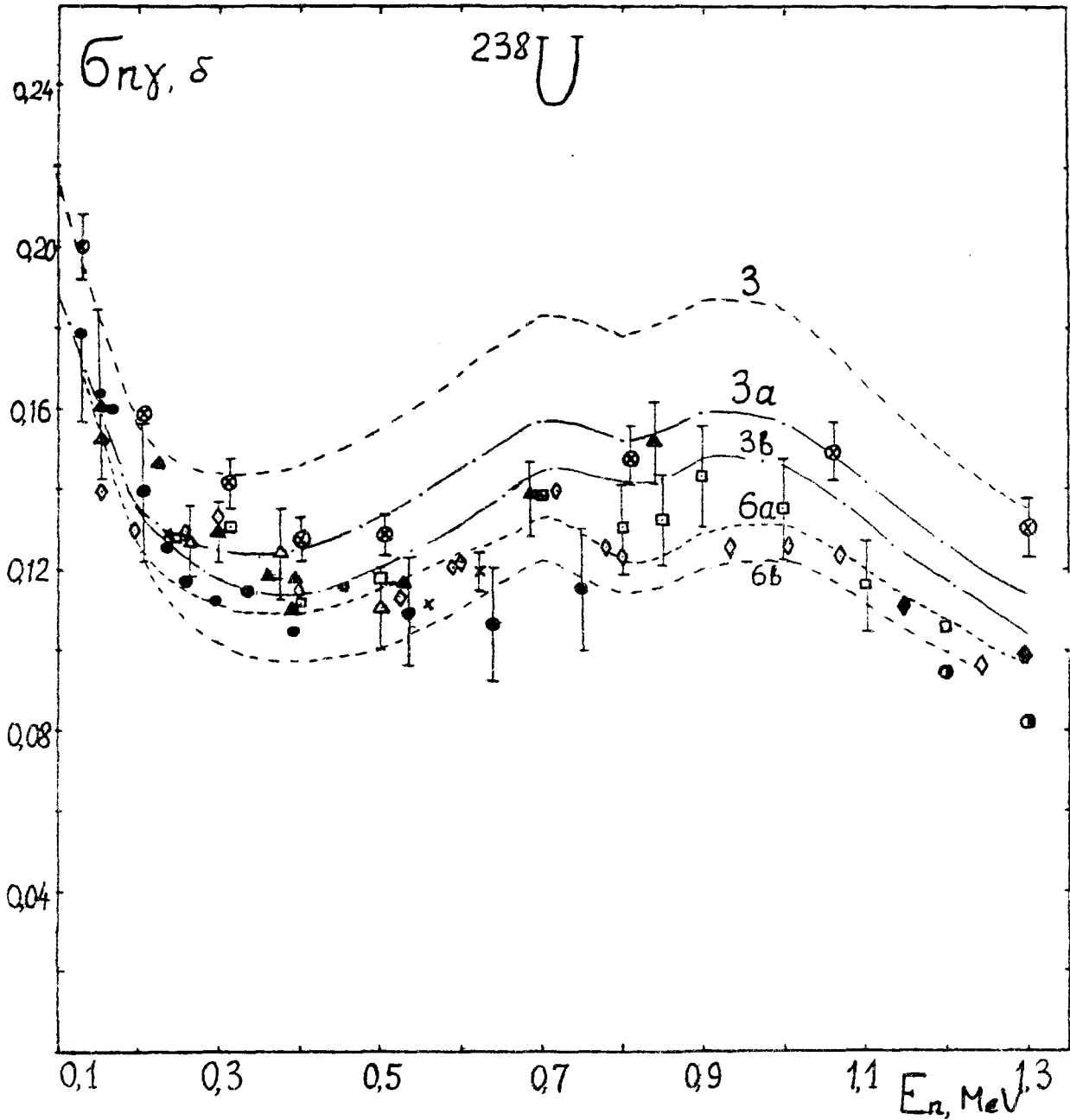


Fig. 4 Comparison of the experimental and predicted data for  $\sigma_{n\gamma}(^{238}\text{U})$  (curve 3, level density Fermi-gas model with collective modes, Lorentz factor,  $\langle D \rangle = 17.7$  eV; curve 3a, the same as for curve 3 but  $\langle D \rangle = 20.8$  eV; curve 3b, the same as for curve 3a but  $T_n$  is obtained with the deformed potential; curve 6a, superfluid nucleus model with collective modes, Lorentz factor,  $\langle D \rangle = 20.8$  eV; curve 6b, the same as for curve 6a but with the deformed potential).

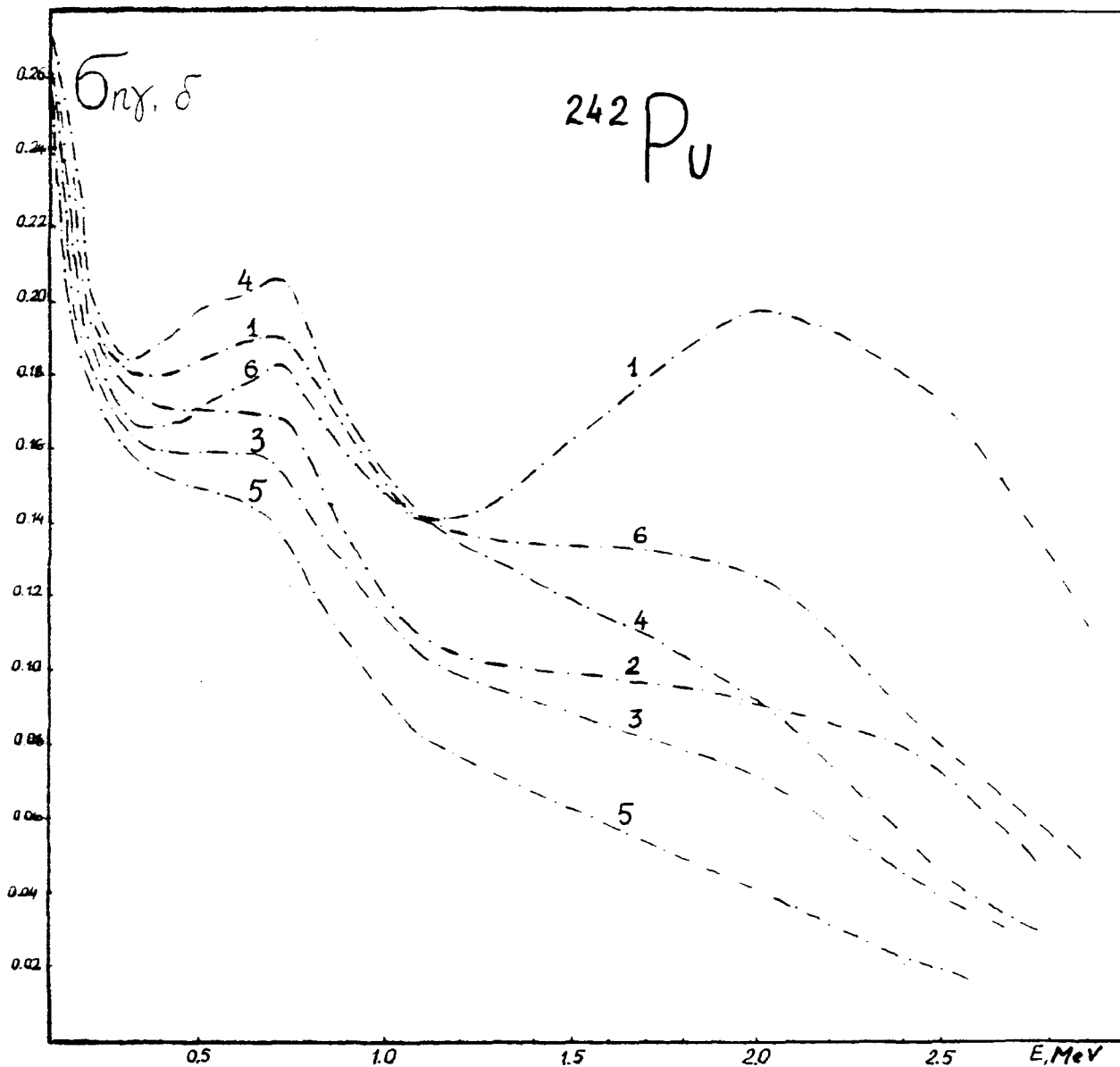


Fig. 5 Predicted data for  $\sigma_{n\gamma}(^{242}\text{Pu})$  (curve 1, level density Fermi-gas model, Lorentz factor; 2, Fermi-gas model, Weisskopf factor; 3, Fermi-gas model with collective modes, Lorentz factor; 4, superfluid nucleus model with collective modes, Weisskopf factor; 5, Fermi-gas model with collective modes, Weisskopf factor; 6, superfluid nucleus model with collective modes, Lorentz factor).

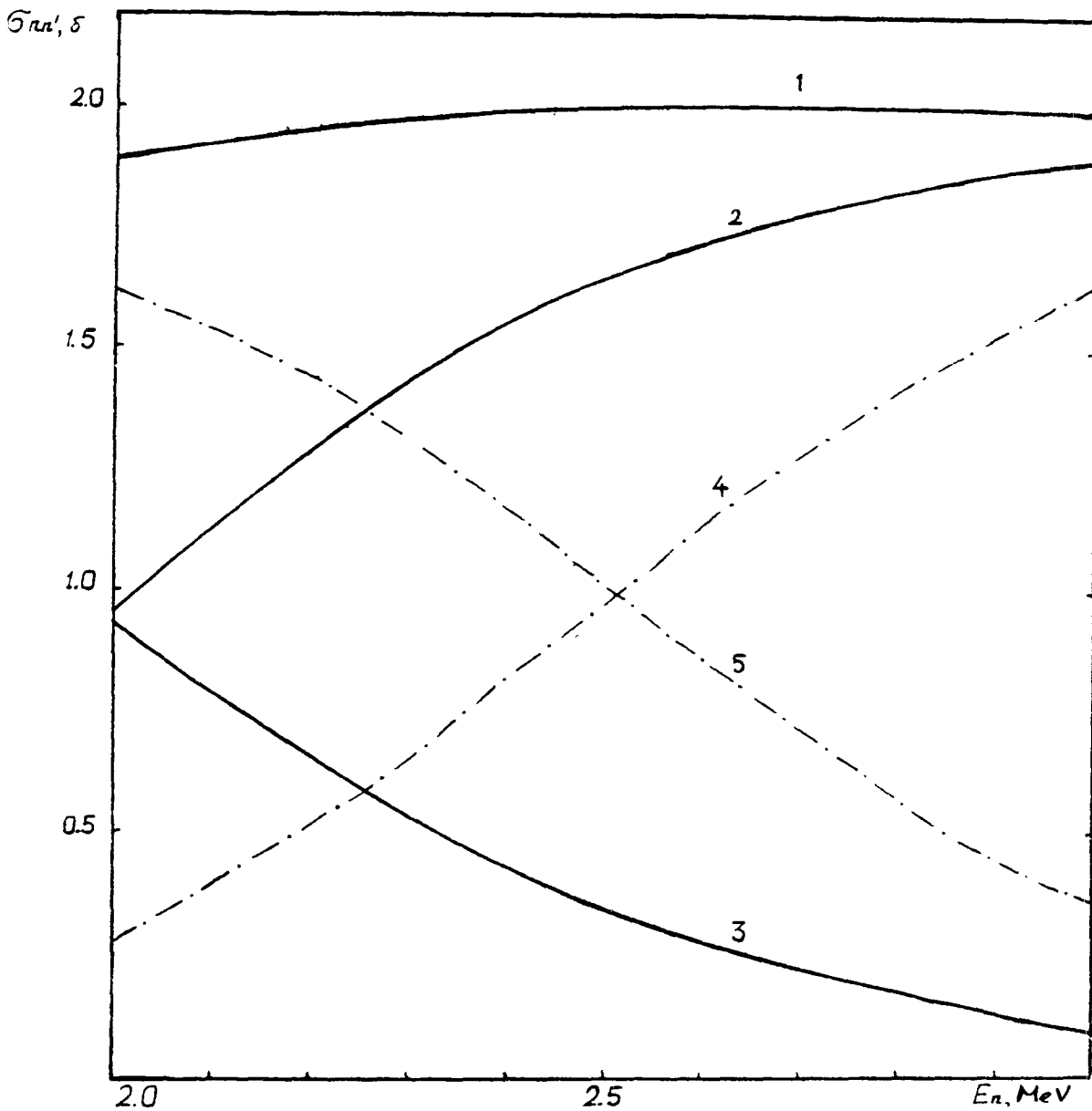


Fig. 6 Level density effect on  $\sigma_{nn'}(^{242}\text{Pu})$  calculation (1, total  $\sigma_{nn'}$ ; 2,  $\sigma_{nn'}$  cont, by the Fermi-gas model with collective modes; 3,  $\sigma_{nn'}$  disc, by the Fermi-gas model with collective modes; 4,  $\sigma_{nn'}$  cont, by the Fermi-gas model; 5,  $\sigma_{nn'}$  disc, by the Fermi-gas model).

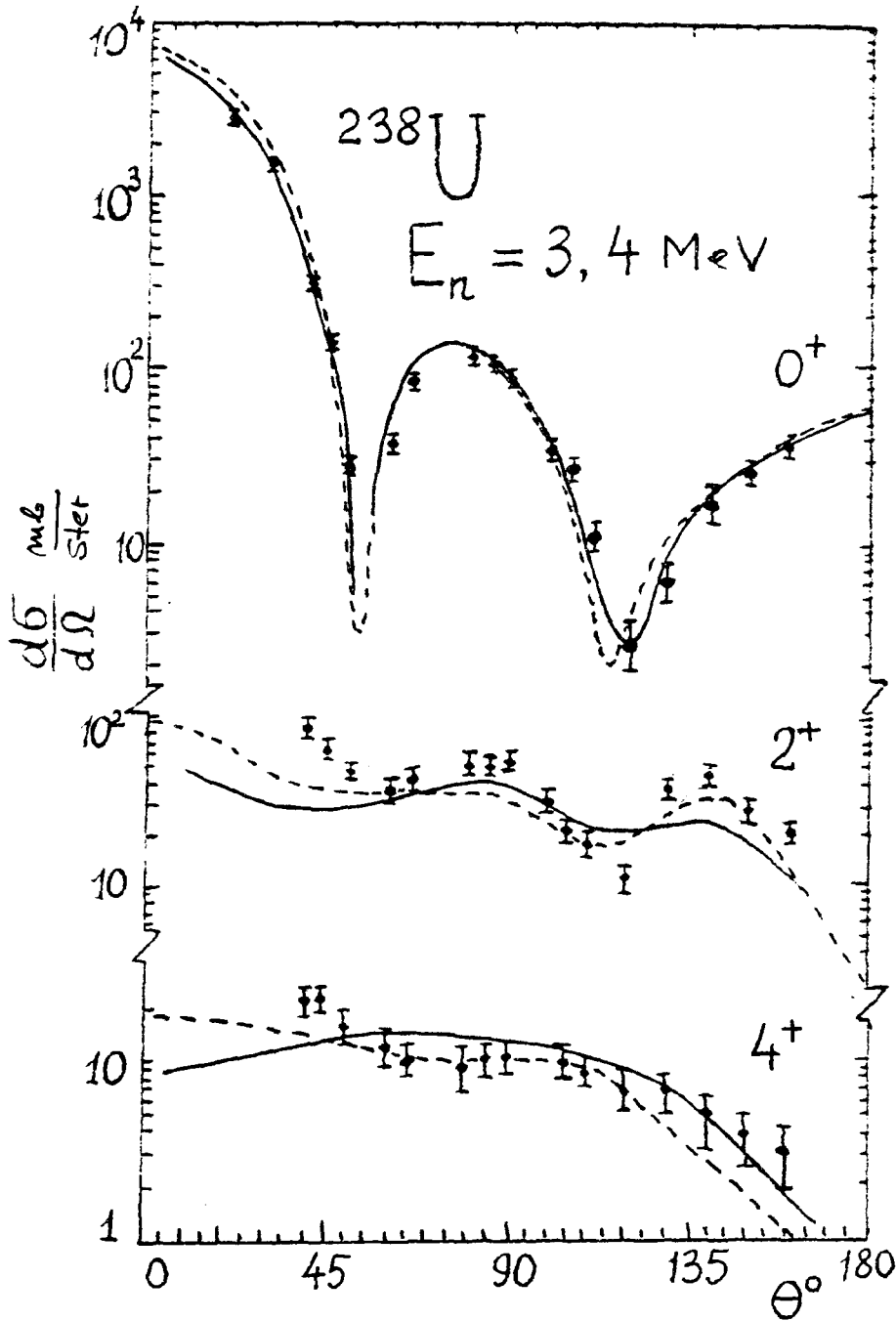


Fig. 7 Comparison of the predicted and experimental data for neutron scattering cross section at  $E_n=3.4$  MeV for elastic ( $0^+$ ), first excited ( $2^+$ , 45 keV) and second excited ( $4^+$ , 148 keV) states for  $^{238}\text{U}$ . Solid curve, present calculations; dashed curve, calculation from /24/.